Instrumental characterization and observations of the Sun and the Moon with a scientific dissemination module in microwaves

Adrián Hernández García

Grado en Física - Universidad de La Laguna

Supervised by:

J. Alberto Rubiño Martín

Instituto de Astrofísica de Canarias

Abstract

I demonstrate the use of a commercial antenna to measure the solar and moon emissions in the microwave band 10-12GHz, and how to use the data in order to characterize the properties of these antennas as real and capable astronomical instruments for outreach and amateur astronomers. The data was acquired in short campaigns at the IAC headquarters and the Observatorio del Teide. A strong radioastronomy background was required to understand and complete the work, as well to develop the needed voltmeter, made with Arduino. The observations consisted in sets of time series pointing the telescope at different elevations, in order to characterize the system noise. Further analysis showed that due to the high noise level of the receiver, the instrument can only be used for a limited amount of astronomical objects. But it was good enough to can use this work as a technology testbench and base level of this kind of microwave science at university level. From the personal point of view, it was interesting and laborious to use an antenna system, as well the scientific dissemination module that it is, and for what it was created within the framework of the internships at IAC in the final part of the physics degree at Universidad de La Laguna.

CONTENTS

INTRODUCTION

a. Motivation and objectives

This work is the result of the use of an antenna system as a testbench of this kind of technology at IAC/ULL but also as part of the research projects that can be done in the university context. It was necessary to know the specific methods of radioastronomy, such the especial instrumentation, the proper knowledge of how radiation is spreading the sources' energy through the space, and the analysis of the results. This work shows that is possible to do this kind of studies in a degree level, with the appropriate materials and procedures run by teachers.

Dr. J. Alberto Rubiño with Dr. Alfred Rosenberg and Dr. Roger Hoyland were the scientific leaders on a previous design of a suitable antenna as scientific dissemination module in microwaves; within the framework of external practices at Instituto de Astrofísica de Canarias (IAC) for the Physics Degree at the Faculty of Sciences, in University of La Laguna (ULL).

Antenna placed at Observatorio del Teide, at the platform of MONS telescope (center) with the solar towers (left) and the radioastronomy area (right), where QUIJOTE microwave project is being developed.

This antenna is capable for getting the Ku band on the microwave spectrum, at 10-12 GHz, just the same than the first instrument of QUIJOTE Experiment, at Teide Observatory. This let us to manage the band used for WiFi, GPS or commercial satellites; that is not any especial part of the spectrum that a student get used to study at university, and could provide us another level of approaching to the science done in it. Then, supported by the few previous studies, a study of how to use this antenna and how to use it in order to achieve actual data of solar microwave effective temperature was chosen. It was necessary to develop an instrument able to register the data, and a complete module for the whole system.

The Sun has a well-known spectrum in all wavelengths, and the intention is to measure the 10-12 GHz band, in microwaves, using new instruments and detectors. From previous study by Zirin et al. (1991)[1], I learnt that this microwave emission comes from the coronal but mostly chromospheric emission. And like it is in the radio spectrum, we are also trying to measure the temperature of this chromosphere, with all the previously learnt knowledge in radioastronomy. The Sun by itself, as the Cosmology, are two of the most important study fields at Instituto de Astrofísica de Canarias. As a student, radioastronomy is the opportunity to get into those both not so close fields.

The objectives of this work are:

1. Characterize the response of the instrument, by measuring the RMS and Mean values in different elevations for noise studies purposes.
2. Characterize the Power Spectrum of the data.
3. Check if the Radiometer Equation is satisfied in the context of this project.
4. Calculate the knee frequency of a set of QUIJOTE data and our own antenna.
5. Carry out transit observations of astronomical sources and develop the software to analyse them.
6. Take solar effective temperatures in function of known lunar calibrated temperatures and determine the phase of the solar cycle where we are.

b. Radiation fundamentals

i. Basic definitions

The specific intensity, or spectral brightness, of an astronomical source is the flow of energy per unit time, area, frequency and solid angle. It can be understood as its power diluted per unit of area, frequency and solid angle.

$$I_\nu = \frac{dE}{dt}\left(\frac{1}{\cos\theta\, d\sigma\, d\Omega\, d\nu}\right) = \frac{dP}{(\cos\theta\, d\sigma)\, d\Omega\, d\nu} \quad [W\, m^{-2}\ Hz^{-1}\ sr^{-1}] \qquad \textit{(EQ. 01)}$$

When measuring the signal, we use an antenna with an specific area. Thus we can obtain a measurement of the called flux density S_ν that is the specific intensity integrated over the solid angle subtended by the source. Taking $\cos\theta \backsimeq 1$ for the majority of astronomical sources, we have:

$$S_\nu = \int_{source} I_\nu(\theta,\phi)\cos\theta\, d\Omega \approx \int_{source} I_\nu(\theta,\phi)\, d\Omega \qquad \textit{(EQ. 02)}$$

This flux density has units of Watts per unit area and frequency, and is usually measured in Jy (Jansky). This is the name of the pioneer radio astronomer Karl Jansky that showed the existence of an extraterrestrial radio signal that did not come from the sun, but from the galaxy center. The definition is: 1 Jansky = 1 Jy = 10^{-26} W m^{-2} Hz^{-1}.

Finally, the Brightness Temperature T_B is the temperature a blackbody in thermal equilibrium would have in order to replicate the observed Spectral Brightness of an object at a given frequency. In this way, for any source:

$$T_B = \frac{h\nu}{k}\, ln^{-1}\left(1 + \frac{2h\nu^3}{I_\nu c^2}\right) = \frac{I_\nu c^2}{2k\nu^2} \qquad \textit{(EQ. 03)}$$

where the final result is in terms of the Rayleigh–Jeans approximation. Citing the NRAO ERA course[7]: "Brightness temperature is just another way to specify power per unit solid angle per unit bandwidth in terms of the Rayleigh–Jeans approximation".

ii. Atmosphere transparency

The atmosphere has different values of transparency/opacity, letting us see different depths depending on the frequency of observation. There are two observing windows located on the visible and radio parts of the spectrum. Thus, at radio, for wavelengths bigger than a meter we do not have nearly any absorption. This absorption is about 0.01 at our 10 GHz frequency band, mainly made by the water-vapor molecules or water combined with other elements. Typical atmospheric conditions in this band appear in the radio data as an additional noise component.

iii. Mechanisms of radio emission

There are a lot of different fields of study with radio waves, from Solar System bodies to the Cosmic Microwave Background. Thanks to the transparency at radio, we can investigate on how galaxies or quasars are, how they evolve and what are their environments, in a wide space-time scale. Leaving aside the radio signal from our Sun, inside the Milky Way we are provided of a lot of places where relativistic electrons provide us a synchrotron radio emission. Those are supernova remnants or pulsars with nebulae. Outside the galaxy there are exotic objects as supermassive black holes, in which surroundings the material is emitting strong radio signals as well.

c. Thermal emission of the Moon

The Moon is our natural satellite. As the minor objects of the solar system, it is not producing its own light, but reflects sunlight. In the case of optical light, we observe it from the Earth with an albedo of 0.136. However, in the radio and microwave bands, we observe the thermal emission from the Moon surface which was heated by the Sun illumination. Its emissions works as a black body, with a high absorption also due to said albedo. In microwaves, this black body radiation comes out showing a moon temperature of around 240 Kelvin, that also depends on how it is illuminated by the sunlight, i.e. how the phase is. This phase variation can be expressed in the following equation by Gorenstein and Smoot (1981)[2]:

$$T_{Moon}(\nu \sim 10GHz) = (202.0 \pm 7.5)K + \left(27.0^{+5.1}_{-2.5}\right) * \cos\left(\varphi_M - 41º \pm 3º\right)K$$

(EQ. 04)

The absolute temperature might be slightly different at higher frequencies, but the previous equation can show us the dependance on the relevant parameter. It has a constant value modulated by a unphased term that also depends on the moon phase φ_M with an amplitude slightly greater than a 13%. But the most interesting result of the equation is that shows in the -41º±3º phase gap that the Moon could be glowing also at lunar night, because of the remnant heating there, when sunlight has gone.

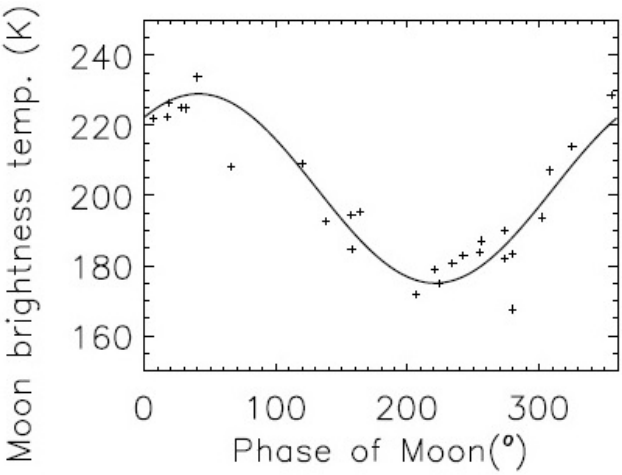

Figure 1: Fit of Harrison, Rubiño et al. (2000)[6] of the Moon Brightness Temperature all over the phases cycle, with data and model given by Gorenstein and Smoot (1981)[2]

For our purpose this equation was useful to understand how are the black body thermal effects working under the regolith upper layer of the moon surface. Thus, after being stored, this microwave radiation comes out as a thermal emission, as an effect of thermal inertia.

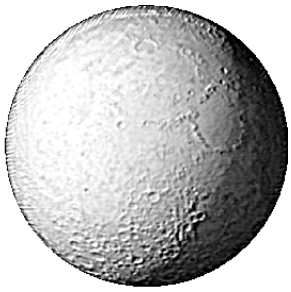

Figure 2: Mostly phase-dependent and homogeneous thermal emission image of the Moon taken by JCMT at ν=350GHz taken from the NRAO ERA course (2016)[7]

d. Solar Radio Emission

The Sun is the brightest radio source seen from Earth. Its emission in optical wavelengths can be described by a blackbody as well, but this is not the case for its radio emission. The following figure taken from 'Radio Astronomy' book by J. D. Kraus shows the solar emission from ultraviolet until radio signals.

The incoming radio signal proceeds from higher altitudes than optical light, showing us a bigger Sun at radio wavelengths, but also by this reason is giving us information about a hotter layer on the solar atmosphere, where we can measure dozens of thousands of Kelvins, but not the 4800-6000ºC that an optical image can provide us.

This excess in radio emission is the result of the 'free-free' braking radiation of the solar plasma, commonly named bremsstrahlung, from the German words 'bremsen' "to brake" and 'strahlung' "radiation". Their free particles have this braking effect comes from the deviation of free protons and electrons on the plasma, when they pass very close to other free particles almost colliding with them. This loss of kinetic energy of particles, transforms into a continuum spectrum of photons with our radio frequencies.

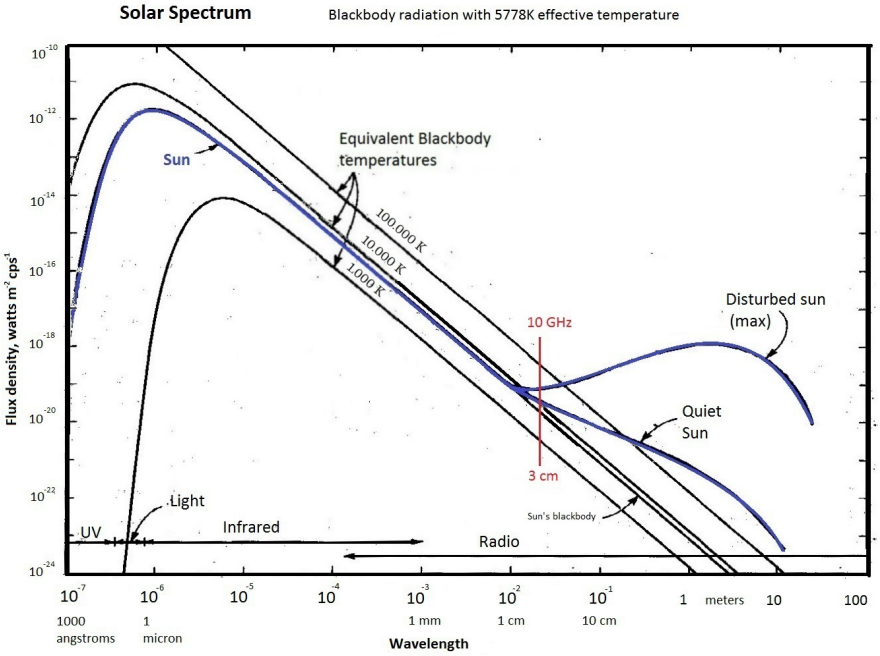

Figure 3: Adapted image of the solar spectrum from the book "Radio Astronomy" by J.D.Kraus (1966)

We can observe in the figure that there is a difference between the blackbody model of the Sun, with Teff = 5778 K, and the real Sun Spectrum in blue, but only at wavelengths longer than ~1 cm, or frequencies lower than 30 GHz. This allow us to observe the variability due to solar magnetic activity in this part of the spectrum.

I have added a vertical red line showing our 10 GHz band (3cm) in which we have a small change between the full disk of the quiet Sun, and the disturbed case. It can show us an estimated value of the expected signal.

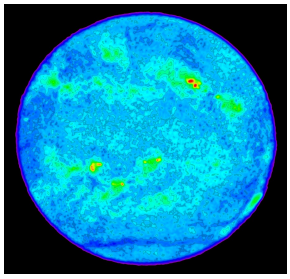

Figure 4: Full disk image of the quiet Sun taken by VLA at ν= 4.6GHz, taken from the NRAO ERA course (2016)[7]

Due to the shown solar emission variability at 10 GHz, we are capable to have an estimation of how the magnetic activity of the Sun is, and then in which part of the activity cycle we are; using our 10-12 GHz antenna.

Table 1: Summary of data from Zirin et al. (1991)[1] for Quiet Sun

Frequency [GHz]	Temperature [K]
9.4	12200 ±600
10.6	11300 ±500
11.8	11000 ±500
13.2	10800 ±500

From the study of Zirin et al. (1991)[1], the expected Sun temperature nearest to our bandwidth, at 10.6 GHz in the quiet phase is around 11300 ±500 K, and is the resulting emission of the bremsstrahlung in the chromospheric and coronal layers.

e. Antenna fundamentals

Like Maxwell's equations are valid when time is reversed, every antenna could be understand as a receiving device or as a transmitting system. This is the Reciprocity Theorem, but we have also the stronger version. This other shows that when a voltage is applied to an antenna A (with measured current) we can measure in another antenna B, an equal current will appear at the terminals of A if the same voltage is applied to B. This Strong Reciprocity Theorem can provide us a relation between two different antennas such that:

$$\frac{V_A}{I_B} = \frac{V_B}{I_A} \qquad \textit{(EQ. 05)}$$

i. Antenna's main beam

For our purpose, we want to know how precise is the antenna pointing to any source. In order to do it, we will obtain the main beam of response, in which we have the main part of the Power Gain pattern of the antenna $\boldsymbol{G}(\theta,\phi)$. Normally this pattern has a main beam along the boresight axis, but also a number of side lobes transmitting a lot of stray radiation into the system. The sidelobes noise contributions, outside the main beam, are illustrated in the following figure. They can be receiving signal from a very far away angular distance. They also can be minimized using directional antennas, as the usual parabolic dishes or horn-shaped waveguides.

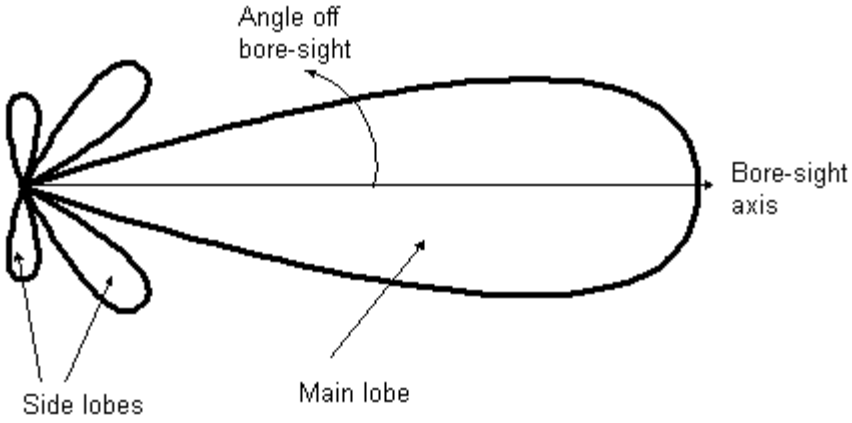

Figure 5: Image of sidelobes asides the main lobe in the power pattern of an antenna, taken from ASAR user guide, ESA[8].

ii. Antenna Temperature - T_A

This concept corresponds to the temperature of a hypothetical resistor at a noise-free receiver that can generate the same output power (per unit bandwidth) at the output of the antenna, at a specified frequency. However, this 'temperature' has to be considered like the sum of different components all over the main antenna system, in that way from (EQ.01) it must have inside the measure of our source signal also.

Thus, the source signal has in addition the components of the detector and losses at the antenna, any radio emisor nearby, the various Earth radio emissions and a background that comes from our galaxy and also from the Cosmic Microwave Background, all these put into a global atmospheric component. We can see all them as follows:

$$T_{Ant} = T_{Source} + T_{Atm} + T_{Rec}$$
$$T_{Atm} = T_{Spill} + T_{Sky} + T_{BG} \qquad \textit{(EQ. 06)}$$
$$T_{Rec} = T_{Loss} + T_{Det}$$

With the general definition of the antenna temperature, we have that it is equal to the brightness temperature pattern of the source, integrated along its angular size, divided by the integrated angular field of view of the antenna. Thus:

$$T_{Ant} = \frac{\int G_B(\theta,\varphi)\cdot T_B(\theta,\varphi)\cdot d\Omega}{\int G_A(\theta,\varphi)\cdot d\Omega} \qquad \textit{(EQ. 07)}$$

where G_B and G_A are the angular coordinates of the source and antenna.

In the limit that $\boldsymbol{\Omega}$ Source $\ll$ $\boldsymbol{\Omega}$ Antenna, we can assume that the brightness temperature is constant into angular parameters. It is an adequate approximation because for the subtended solid angle of almost any astronomical source, will be less than our expected 3 degrees of field of view at our antenna (taken from the antenna's manufacturer). Summarizing the concept, we will get our source, the Sun brightness temperature $\mathbf{T_B}$, but diluted into our main beam. By this reasoning we arrive at the following equation:

$$T_{Ant}^{Source} \simeq T_B^{Source} \cdot \frac{\Omega_{Source}}{\Omega_{Ant}} \qquad \textit{(EQ. 08)}$$

iii. Measuring the signal

Our antenna is part of an electrical circuit. In this scheme, the antenna temperature is the source of a Johnson-Nyquist noise, formally 'thermal noise', and can be understand as the generated by thermal agitation of the charge carriers, according to:

$$< V^2 > \; = \; 4\, k_B\, T \cdot R \qquad \textit{(EQ. 09)}$$

where the left term is the mean square of the voltage variance per hertz of bandwidth, k_B is the Boltzmann's constant, T is the absolute temperature of the equivalent resistor, and R is the resistor value.

The antenna temperature provide us a voltage proportional to this system temperature T_{Sys}, but also to the system Gain, expressed logarithmically in decibels (dB). So if we can measure and control the system gain G, we can have the result voltage at our data. This AC voltage will be transformed into DC voltage V, and then be measured in a voltmeter.

$$V \propto T_{Sys} \cdot G \qquad \textit{(EQ. 10)}$$

However we will have a lot of new contributions on the signal; namely AC noise on the energy source, other AC and DC signals into different equipments, etc. In this situation, we are especially well positioned because we are using an electrical detector; and we can treat these different signals as independent in our measure. Thus, we can easily compare the voltage obtained pointing at the source, with a non source signal, and then have the Source Signal Voltage as the rest of them. Using DC voltages, this will bring us a couple of starred parameters on any voltmeter instrument: the Main Gain (with the main value of the voltage) and the Offset of this voltage, that is our baseline in order to measure rise and fall of these voltage values, as real variations in the source signal.

Finally, this DC voltage will be converted into system temperature, and then into the source's brightness temperature as we have just seen in the previous sub-sections. Thus, here we have the summarized concept of the instrumental acquisition:

The main beam of the antenna provide us a AC voltage that behaves as a thermal noise on our circuit, which when converted into DC voltage at the detector, is amplified and finally saved on the instrument. In this voltage is stored the antenna temperature, and adding the power dilution of the solid angle of source into our beam, we can obtain the brightness temperature of our source.

iv. Radiometer equation

The radiometer equation is the Signal to Noise relation applied for the radioastronomy case. The radiometer equation gives a relation between the standard deviation ΔT_{RMS} at a data set, and the average system temperature T_{Sys} by the application of some given parameters: Δ_ν as the bandwidth of the instrument, τ the sampling rate, G the gain, and ΔG the gain variations. Thus, the equation shows us the noise contributions as the two addends on the right part of the root, as it is shown on the following equation:

$$\Delta T_{RMS} = T_{Sys} \sqrt{\frac{1}{\Delta_\nu \tau} + \left(\frac{\Delta G}{G}\right)^2} \qquad \textit{(EQ. 11)}$$

The ideal radiometer equation corresponds to the case $\Delta G=0$.

2. METHODOLOGY

Our goal is to measure the solar radio emission at 10 GHz. For this purpose, the Moon is used as a calibrator. We first describe the instrumentation used in this work, the main antenna and radiometer system.

a. Instrumentation

A brief summary of the instrumentation consists of: An antenna (*i*) mounted on an amateur telescope mount (*ii*). These as well are combined with a IAC provided main detector (*iii-3*) and later an amplifier (*iv-1*) in order to be recorded by an Arduino Yún board[13] (*iv-3*) that had to be chosen and programmed with a specific voltmeter code to work as our main recorder (*iv-4*). All this material into a designed plastic reused briefcase, working as a homemade radiometer (*iv*). All this systems were funded by the Instituto de Astrofísico de Canarias, as leaders of the previous project: the design of the same system, as a scientific dissemination module in microwaves for all audiences.

i. Antenna dish and system

The mere photon counting technique to reconstruct the intensity of the emitted signal is not useful in Radio Astronomy. Photons are too weak to detect them individually (λ = 1m (300 MHz) $\Rightarrow$ 1.2 × 10-6 eV). By contrast, it is necessary to measure the incident electric field. Parabolic antennas are designed to focalize plane waves of any radio signal traveling in the direction of the optical axes of them. Ours it's a 110 cm offset satellite antenna of Tecatel brand. With 10.7 Kg, it has a 1000x1100mm dish of galvanized steel with a epoxi-polyester thin hedge layer. Within we have our LNB (*iii-1*) first detector located just in the forward direction in the pole, but not blocking any signal thanks to this offset design; and also our sound finder (*iii-2*).

ii. Equatorial mount

In order to properly point the antenna to any astronomical source, we used a typical amateur polar mount. Its german equatorial design let us put the antenna in one side of the right-ascension axis, and the counterweight in the other side, both rotating around the declination axis. A Vixen SXD model, from Sphinx Deluxe version, was chosen. It is a big and strong mount able to load big telescopes, or antennas like we do. This model comes with an almost total control of the speeds of the different movements, but like it's also popular enough, we can find on the internet the appropriate driver to could control it from a computer.

iii. Detectors

1. First detector - LNB

Low Noise Block (LNB) is the first device that receive microwave signals from the source collected by the antenna's main dish, then amplifies it, and later downconverts the bandwidth of frequencies to a lower block of frequencies. The downconversion effect let us put the signal into a coaxial cable, a practical result in order to manage it.

2. Sound finder

The sound finder is actually a commonly used satellite finder, in order to locate the signal of any communications satellite in geostationary orbit. Ours is provided with an analog meter and sensitivity potentiometer, with them we can realize when are we really pointing to a powerful source, instead of only using the mount's computerized system, with its different errors, nor only pointing manually.

3. Main detector provided by IAC

It takes AC input into DC output (shown at following figure 6). It has attached to DC filter that blocks all DC signals into the main antenna circuit, letting only AC source's signal enter inside the detector. Such a system was required to separate DC energy system and signal system in the same cable set. This DC filter and AC detector, in scale of microvolts, was provided by IAC's electronic workshop and managed by Roger Hoyland as engineer in QUIJOTE project.

iv. Radiometer

A plastic briefcase in disuse, made for telescope pieces was taken as container of detectors and most of the electronic system. Actually it was finally use as main instrumentation system (figure 7) and it can be developed as a entire integrated instrument. Here I want to emphasize the perspective on promote the reuse of obsolete parts on science also.

1. Amplifier

As well with the AC detector, this piece was provided by QUIJOTE's IAC project, and reused because it was an obsolete one. It has 3 channels in order to give an amplified signal output around 1-5 millivolts, stronger than the previous microvolts and strong enough to can be registered in the later control board. The output can be tuned in Gain and Offset in order to control the starting point of the electronic system at any time. The difficult challenge of this amplifier board, was to feed it, since it needed +12V and -12V power inputs without a common ground level, necessitating the use of two independent 12V batteries.

2. Power supply

For the above, and to reuse materials, 2 old packs of 8 battery holders were used. They were feeding the previous amplifier, the inverted polarity mount, the antenna itself and the Arduino board with a 12V to 5V reductor.

3. Arduino board

"Arduino is an open-source electronics platform based on easy-to-use hardware and software." In this sense, 'Arduino Yún' board[13] is a complete model with WiFi, SDcard, its own linux OS, and ports as Ethernet and the common USB-A and microUSB, all integrated. These components are unusual in other Arduino boards.

The Yún board is the core of the instrument, of the radiometer. It is the register of the measurements, as a digital voltmeter with special capabilities. It was firstly designed thanks to Juan José Sanabria, a telescope operator and resident astronomer at IAC. He was like an Arduino teacher in every stage. I finally understood the behavior of the whole system and I was able to finish the code by myself. Having to test it and change it a lot due to the different requirements along the study.

The board has analog pins in which we put the antenna signal, pre-processed at IAC main AC to DC detector. We use Ethernet to change and to monitor the working code onboard, that can work without any other connection except power. It uses the SDcard in order to save the data every few seconds. Finally, it has a button installed to switch it on and off, whenever we want; attached to a green LED to show us its status when using offline.

4. Voltmeter Code summary

Arduino software let one create and edit code with its own programming language, based on and similar to C, C++. Our "Yún" board has WiFi, Ethernet and USB connections, to recording the data in the appropriate way. A voltage register rate of 100 milliseconds was decided, as well another of 10 measurements at a buffer to save the data into the SD card. To make actual measurements, the board compares an onboard voltage analog reference, with our signal.[13]

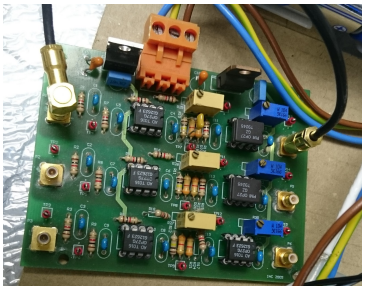

Figure 6
IAC's DC amplifier board

Figure 7
Radiometer briefcase

Figure 8
View of the whole system at IAC (right)

b. Observation campaigns

Table 2: Summary of observation campaigns

#	Date	Main purpose	Place	Comments
0	Dec 18th, 2015	Methods testbench	IAC Headquarters	First solar calibrated temperature
1	Apr 12th, 2016	Observational test	IAC Headquarters	Try to measure the noise
2.1	Apr 29th, 2016	Calibration	Teide Observatory (OT) *	Test measurements
2.2	Apr 30th, 2016 - Morning	Sun-Moon Transits		1 lunar + 1 solar
2.3	Apr 30th, 2016 - Afternoon	Noise study		10x from 0º to 10º
2.4	May 01st, 2016	Sun-Moon Transits		2 lunar + 2 solar continuously
3.1	Feb 4th, 2017	Solar measurements	Teide Nat. Park	3 pairs Sun-Moon attempted **
3.2	Feb 10th, 2017	Electronic noise	IAC Headquarters	Measuring a blank field

(∗) All but one of the OT transit measurements became unable to study, due to a malfunction detected there, for which the radiometer was working in reverse. The smaller the signal, the higher the voltmeter level, making unclear that good data sets were recorded.

(∗∗) It was useless to try to study these measurements as it was almost impossible to discern the Moon signal over the base level. It seemed to be result of the same problem affecting the radiometer system, seen on the OT data sets.

i. Detailed campaigns

In order to minimize the visits to the Teide Observatory, a set of measurements were delivered first at IAC headquarters in order to prepare the instrument and the observational procedure. Of course these first observations at La Laguna were developed as part of one of our goals, the main noise study of the whole system.

1. First noise measurements at IAC Headquarters

It was carried out at 'Plaza de los naranjos', a square in front of Instrumental division inside IAC headquarters. Along the morning of 12th April 2016 it was carried out an especial set-up of the radiotelescope system. It was necessary to point that this square was not facing the North, using a on-site rule as 1 East x 3 South tiles deviation. The front leg of the tripod was placed exactly at 9 East x 8 South tiles from the stairs pillar corner. We put this leg was pointing the North, since this one is over the polar axis of the mount.

Later, the antenna and counterweight bar were leveled and the antenna was mounted on the West side, moving along the astronomical meridian. Finally, the Arduino time was adjusted through the web browser on the computer, via SSH over Wifi, for proper adjusted time of the measurements.

Table 3: Relation of data files - IAC Headquarters

Original name	Main purpose	Exp. Time	Observations
datos_v_prueba_tfg_ino.dat	Noise 0º-90º every π/8 rad 90º-0º Scan at constant speed Noise at around 28º altitude	5x 5 min 1 min 5 min	Elevations taken from an analog level meter Measured speed at about π/2 radians/min Another test one in the latitude notch

2. Transits and Noise data at Teide Observatory

Thanks to an expedition to Teide Observatory carried out with the Astrophysics Department of University of La Laguna, I could accompany a group of students and use the OT facilities at Izaña. It was from Friday, April 28, to Sunday, May 1 2015.

In the first two available hours I set up the antenna and tried to measure the ground level of the whole voltmeter. Although it was almost at sunset, I aimed to the sun in order to check the correct functioning of all systems, and also to calibrate the base level and gain of the amplifier board on the radiometer. At that moment I realized that the system was in malfunction, working in reverse. Instead, I could verify that it continued working in a range of voltages similar to when previously the device worked well at IAC. Later that night I was helped again by Juan José Sanabria some hours in order to fix and solve problems on the data acquisition and the performance of the Arduino system. Finally the system was nearly ready for next morning, but still working in reverse mode.

On Saturday I was using the whole system set up at MONS platform, measured at 28.301250 North and 16.510970 West with 2390 meters above sea level. Along the morning I took calibration test file, but also the first lunar and solar transits, with an exposure time of 40 minutes each one. They were made with a stopped position of the antenna, at 5 degrees into the West of each body's signal maximum. In this 40 minutes, we hoped a natural transit for the two bodies, passing through the center of the antenna in 20 minutes, corresponding to the angular shift made.

I could realize how hard is working at Teide, almost all time under the spring Sun, as tall as 77 degrees. For this reason I tried to take advantage of the registration times to keep some data on the temperature of the radiometer and other on-site tests, which could be useful in the analysis. Some result were that the radiometer was 5 degrees hotter than the environment, when opened. I could also experiment with the faint acoustic signal of the named "sound finder", with which I understood that the antenna must be receiving signal from my body, which I had to take as Spillover signal noise because I was not aligned at all with the direction of the mount.

During Saturday afternoon I came to the system with a better plan than I thought before. Moon had gone, and I decided for elevation noise measurements to make more of them in less time each. Keeping in this way the state of the signal system untouched, maintaining the properties of gain and base level. This could provide us a better quality data and preserve the radioastronomy concepts learnt before. A set of 10 measurements of 10 minutes each was chosen, followed by another scan measure like at IAC.

Since I only had one solar transit and another lunar, I went to take more transits last morning, on Sunday, May 1. As with all setups, after more than an hour of preparation, I was able to start the observations at about 10:20h. It will be again a sequence of lunar and solar transits, with a continuous use of the receiver antenna system, for better quality of data. But keeping each data saved in their own file. Although the day was really good to work, I could only take 2 measurements of each transit, because the final time at Teide was at 12:00h.

During the waiting time of the transits, I went to package my stuff and prepare to leave the observatory. As the final meeting place was close to my position, I took advantage of the last hour for a final data collection, from the sky background in this case, while I was collecting the material of work. It was for having another whole system noise measurement, with the same conditions of the previous 4 transits, that can be affected in a very different way than every other taken previously.

Table 4: Relation of data files taken at Teide Observatory

Original names	Main purpose	Exp. Time	Observations
ot_1_2016_04_30_09_55_29.dat	Natural transit of the Moon	40 min	Displacement of -5º to +5º
ot_1_2016_04_30_10_36_15.dat	Natural transit of the Sun	40 min	Displacement of -5º to +5º
----------	----------	----------	----------
ot_2_2016_04_28_17_51_41.dat	Noise at 10º	10 min	
ot_2_2016_04_28_18_02_35.dat	20º	10 min	
ot_2_2016_04_28_18_13_53.dat	30º	10 min	All with azimut: ~85º
ot_2_2016_04_28_18_24_40.dat	40º	10 min	
ot_2_2016_04_28_18_36_02.dat	50º	10 min	
ot_2_2016_04_28_18_47_09.dat	60º	10 min	
ot_2_2016_04_28_18_58_05.dat	70º	10 min	
ot_2_2016_04_28_19_09_06.dat	80º	10 min	
ot_2_2016_04_28_19_20_40.dat	90º	10 min	
ot_2_2016_04_28_19_34_22.dat	90º-0º Scan and 0º-90º Scan	130 seconds	Constant speed at about $\pi/2$ radians/min
----------	----------	----------	----------
ot_3_2016_05_01_08_48_38.dat	Natural transit of the Moon	32 min	Displacement of -4º to +4º
ot_3_2016_05_01_09_24_19.dat	Natural transit of the Sun	32 min	Displacement of -4º to +4º
ot_3_2016_05_01_10_00_40.dat	Natural transit of the Moon	32 min	Displacement of -4º to +4º
ot_3_2016_05_01_10_35_20.dat	Natural transit of the Sun	32 min	Displacement of -4º to +4º
ot_3_2016_05_01_11_09_41.dat	Noise Calibration Blank Data	32 min	Pointing to northern pole on the sky

ii. Data acquisition and files

The data was taken by an 'Arduino Yún' board[13] and we had to take it from its SD card. We did it without any disassemble of the cardboard box, getting into the system via a the "sancho" WiFi Hotspot and the SSH access from our computer.

In order to get an intelligible format to us, not only readable, but for the later IDL processing program, I chose a double ordered columns format. In order to show the data format, we have the following table explaining a sample of the data saved.

Table 5: Data format

Actual names and data	Explanation
ot_3_2016_05_01_08_48_38.dat	PLACE_SESSION_ YEAR_MONTH_DAY_HOUR_MINUTE_SECONDS.dat
3048650,1472 3048750,1897 3048850,1785 3048950,1662 3049050,980 3049150,1392 3049250,1627 3049350,1355 3049450,1717 3049865,1515	The row on the left is showing a sample of the two columns data saved on our files, in which we have put the time in milliseconds on the first column, and the voltage in millivolts on the second one. We can see the 100ms period between measurements. With the time in the title of the file, that is put from the Arduino time system when pressing the acquisition button, we can adjust the correct time of every single data, but also with the appropriate correction on the moment of data maximum, in which we are on the center of the object (Sun or Moon) we can also shift all times to the correct sidereal time of the measurement.

3. ANALYSIS AND DISCUSSION OF THE RESULTS

In this chapter I present the whole compendium of results obtained at Teide Observatory (OT), at Izaña, and at IAC headquarters at La Laguna (IAC). They'll be presented as graphics and/or numerical results obtained all over the semester.

a. Noise studies

The first goal of the study was the characterization of the different components of noise that our antenna was capable to measure. Radio measurements are mainly affected by the so called Johnson-Nyquist thermal noise, which is statistically a white noise component. In addition, for long integration times, all electronic devices have also a low-frequency component of flicker noise, which in the power spectrum appears with the dependency $\sim A(1/f)^{\alpha}$, and where 'α' typically can take values between 1 and 2. We call this second component "1/f noise".

i. Data files plotted with RMS and Mean values

In the main campaign at the Teide Observatory, there were taken 11 measurements of the signal at equidistant elevations, in order to measure their possible differences and also check the tolerance of the system to work for a long time exposure. The first 10 elevations were divided from 0º to 90º in 10 to 10 degrees, with a total integration time of around 10 minutes each. Here there are the different raw data files, presented with date, time, elevation, signal average and RMS; in figures from 09 to 19:

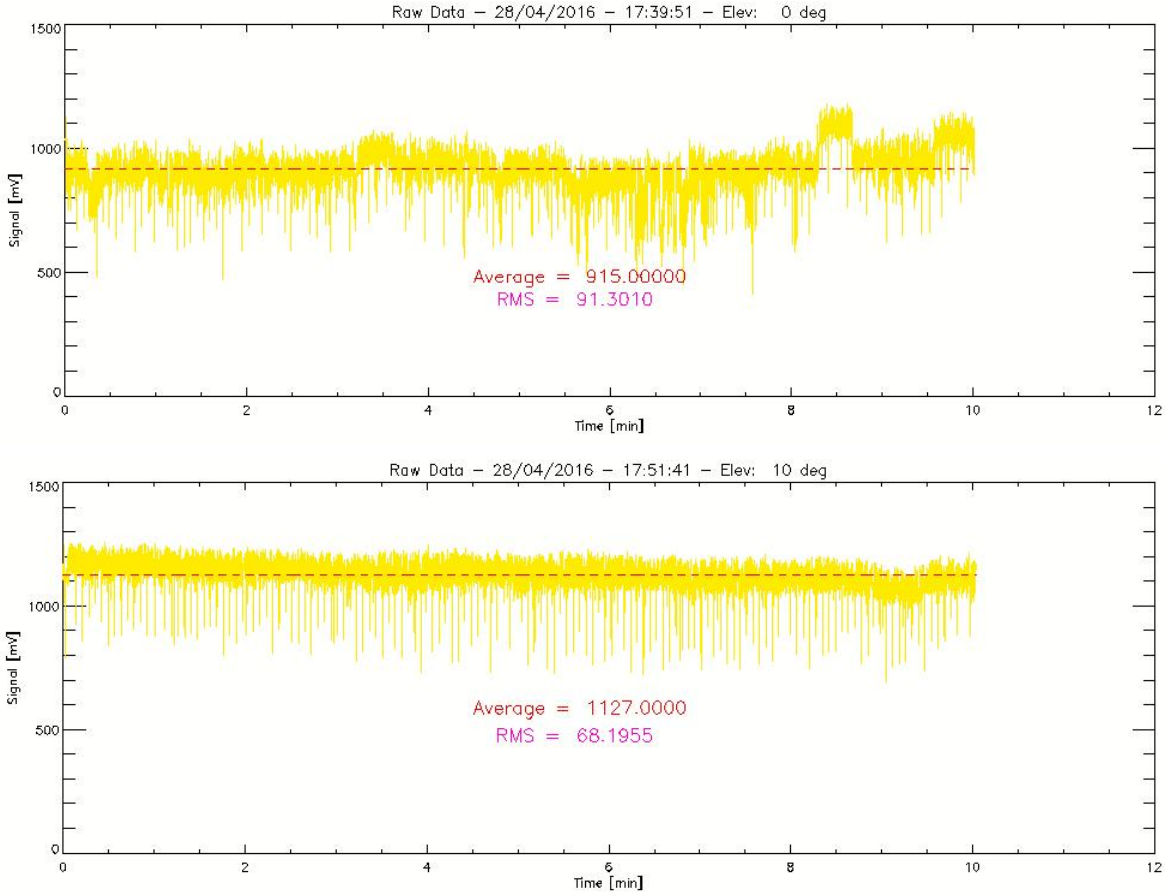

Figures 09 and 10

An increase from figure 10 to the end is observed, due to a malfunction of the radiometer system registered, working in reverse. It had to be greater at 0 degrees than in the rest of elevations, because of the greater contribution of the soil at this case. All the rest of figures show an increase of the average signal, reverse as expected.

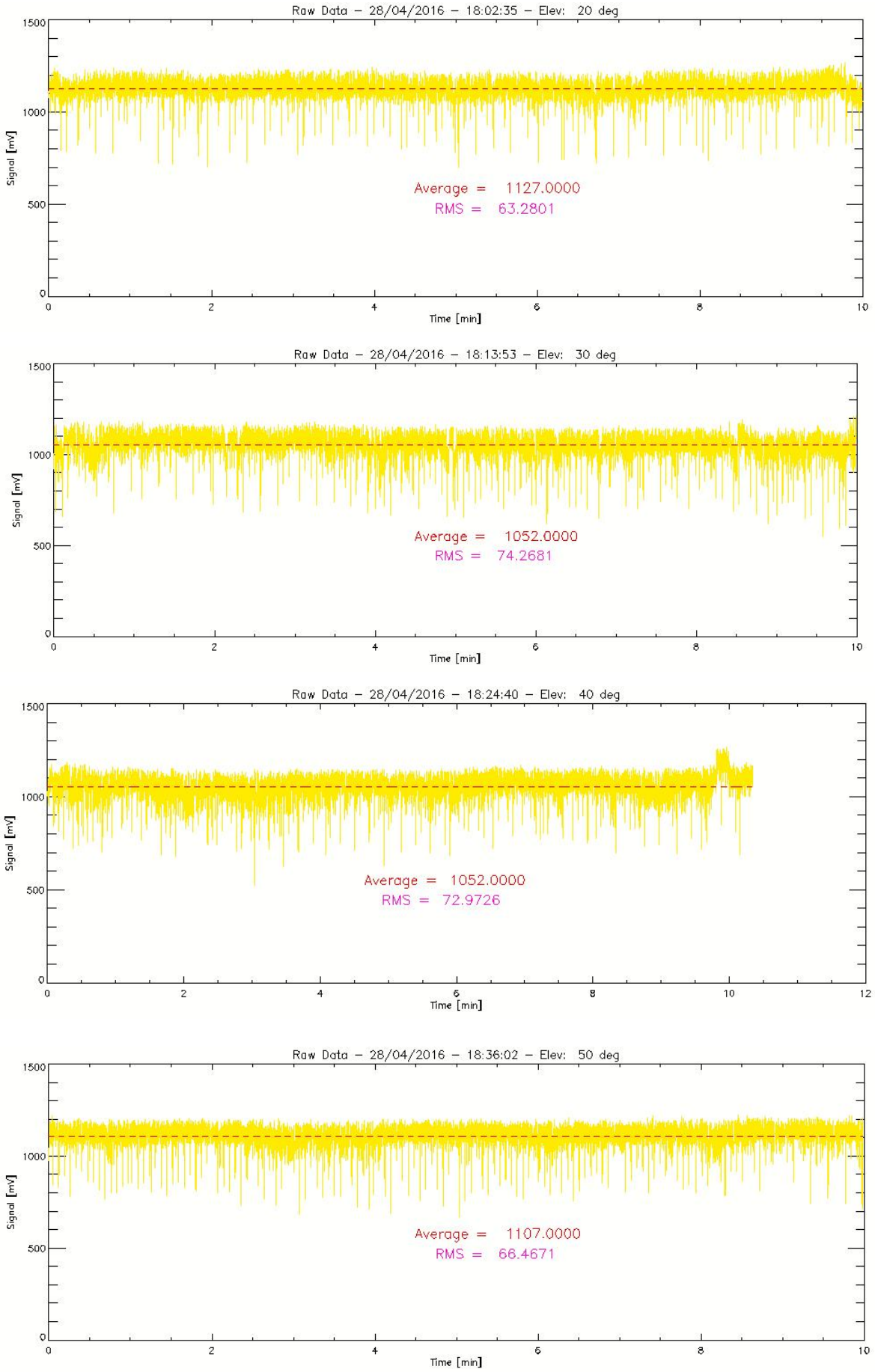

Figures 11 to 14

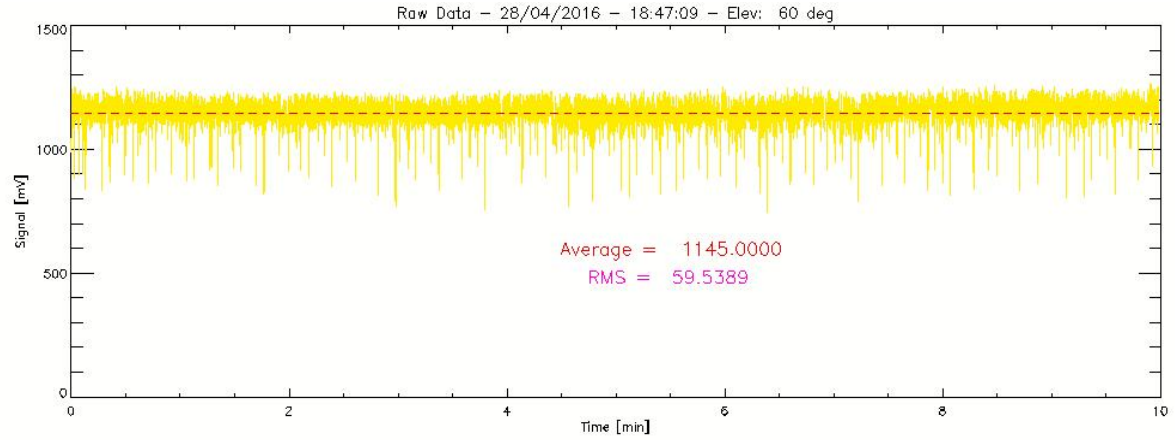

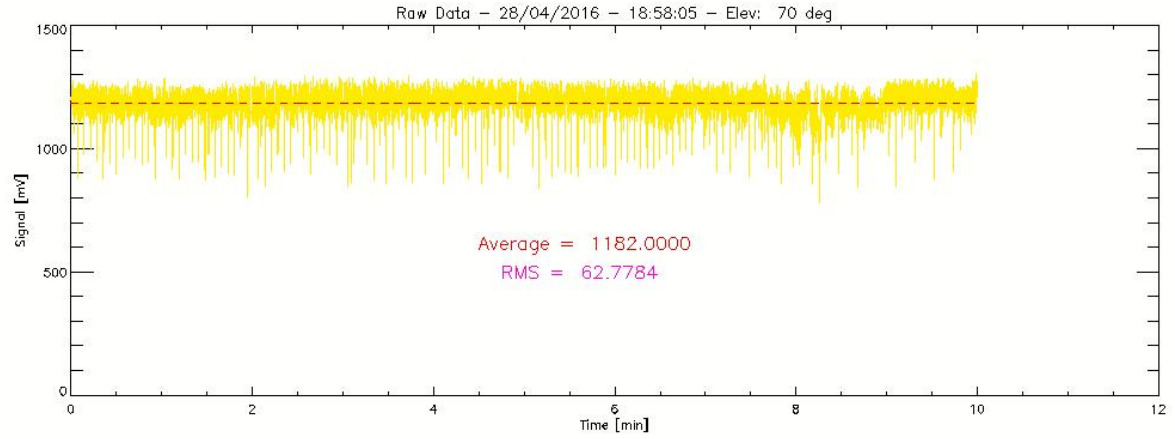

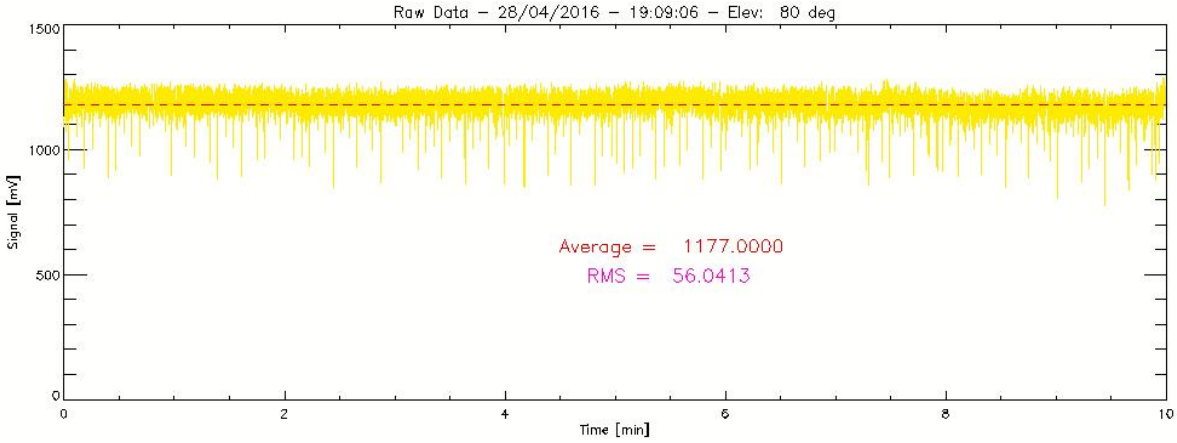

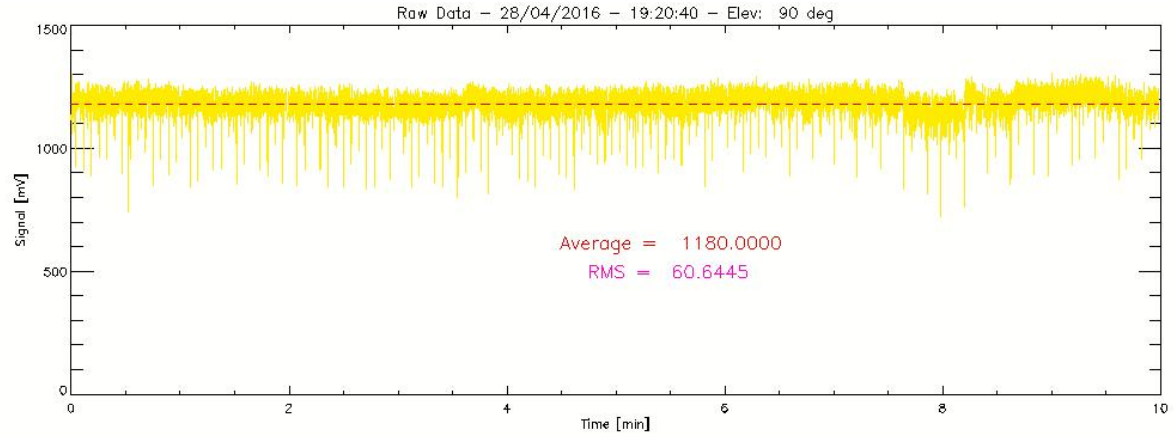

Figures 15 to 18

And a final eleventh measurement was taken scanning the total extension of elevations, from the final 90 degrees to the initial 0 degrees, but coming again into 90 degrees; at a constant speed, moving with the engines of the mount. Here we have the raw data at following figure:

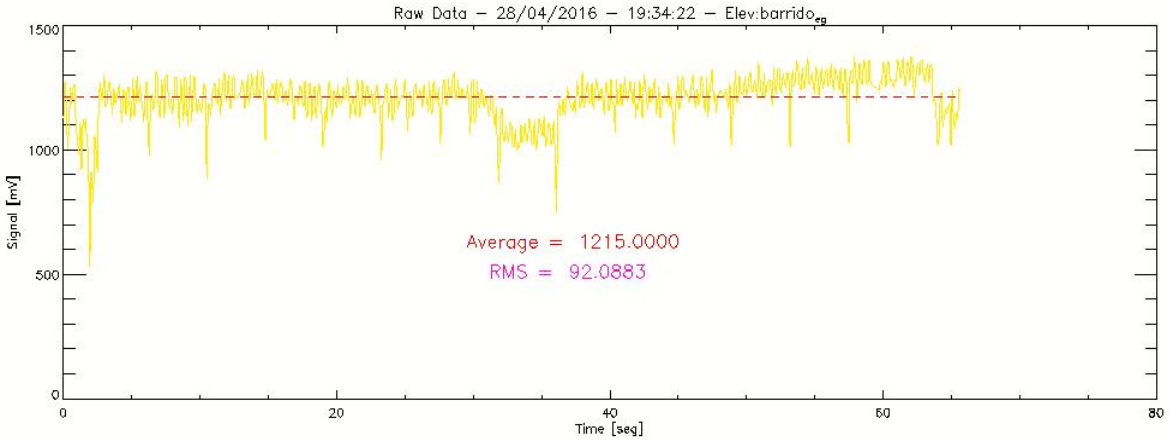

Figure 19

We can see now that the signal is different just in the middle of the scan, working in reverse as it was said before, when the antenna is likely getting ground signal into it. But in the rest of the scan, it is almost flat like the rest of measures. Also appears an increase of the average value from the start to final, thing that can provide us a slight dependence on the atmosphere temperature, as another noise component. Here we have the summary of all the results obtained:

Table 6: Results on elevation measurements

		Data Results			Analysis results	
Date	#	**Integ. Time** [min]*	**Elevation** [degrees]	**Mean** [mV]	**RMS** [mV]	**Derivative** [mV/min]
28/04/2016 17:39 h	1	10.01	0	915	91.30	+5.63
	2	10.03	10	1127	68.20	-7.72
Location	3	10.00	20	1127	63.28	+0.01
Teide Observatory	4	9.99	30	1052	74.27	-0.06
('MONS' platform')	5	10.34	40	1052	72.97	+3.64
	6	9.99	50	1107	66.47	+0.02
Azimuth**	7	9.99	60	1145	59.54	+0.02
ENE	8	10.00	70	1182	62.78	-0.31
	9	10.00	80	1177	56.04	-0.04
Sampling rate	10	9.98	90	1180	60.64	+0.01
10 Hz	11	1.09	Scan	1215	92.09	+0.85***

(∗) The integrated time was achieved using a chronometer.

(∗∗) The azimuth was chosen avoiding any bright microwave source, as the geostationary band of satellites. But also the different contributions that could come from the rest of building facilities at the observatory.

(∗∗∗) The result of the mean derivative value of the eleventh measurement, into the scanning of elevations; was made taking only the first 1 minute of data, from 90 to 0 degrees. Note that the scan is affected by a visible jump in the data at the middle, showing the largest variations (and derivative value) when pointing near to the ground.

ii. Power spectrum of data

Here we have the power spectra of all previous raw data files, from figures 20 to 30. All of them have a similar pattern, but are shown in order to compare them. The power spectra are plotted in yellow color, and another power spectrum of smoothed data in purple, to check some peaks. There are also 3 cosines of 0.01, 1 and 3 Hz each, (corresponding to blue, green and red), added in order to highlight some relevant places over the frequencies axis.

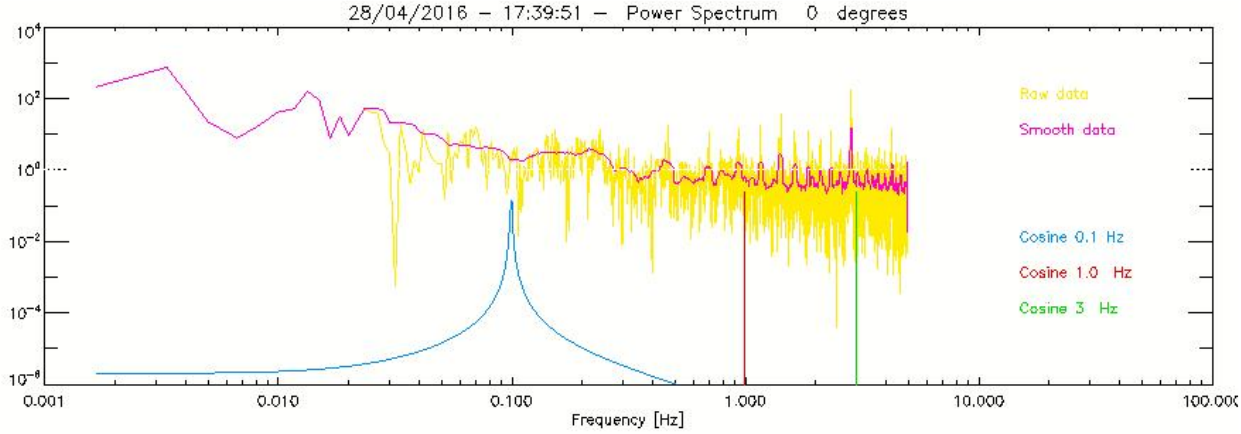

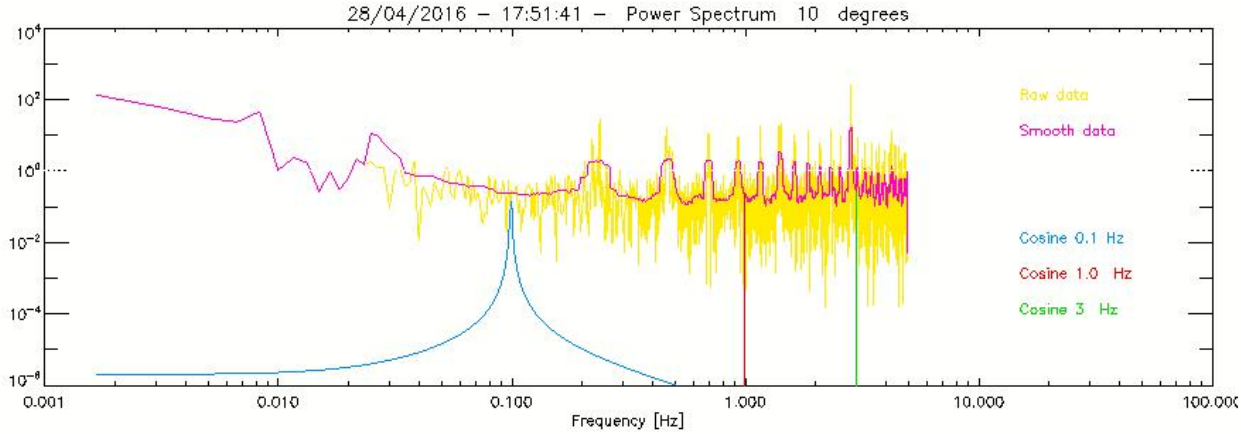

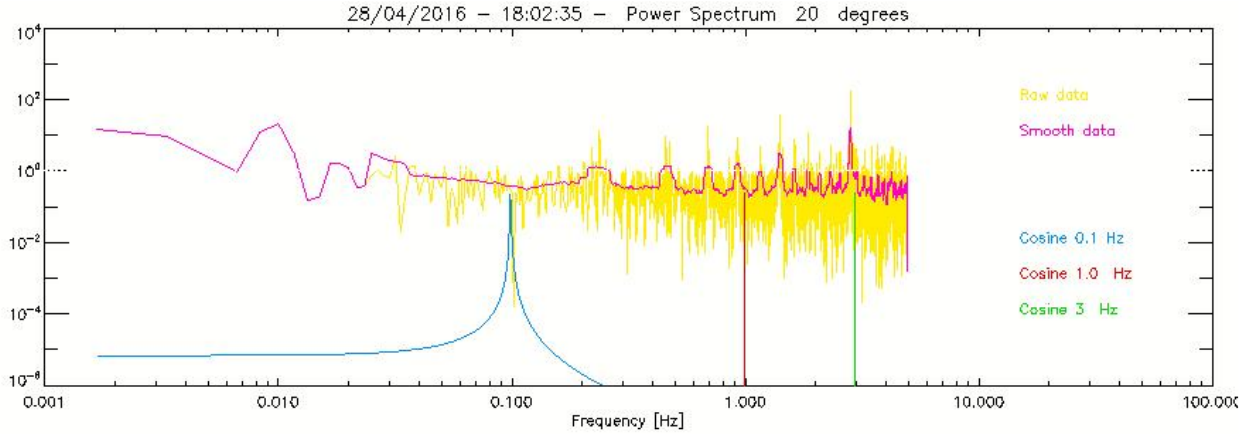

Figures 20 to 22

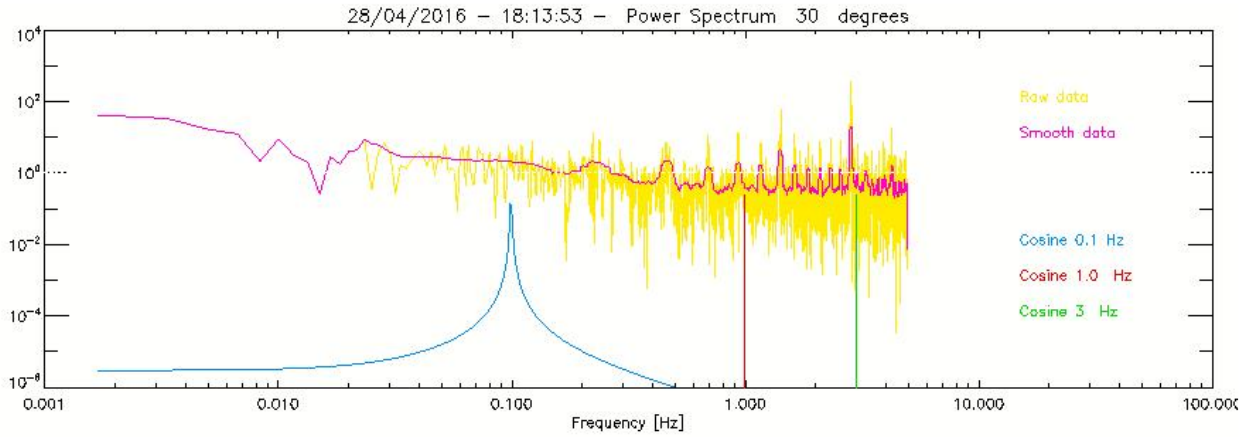

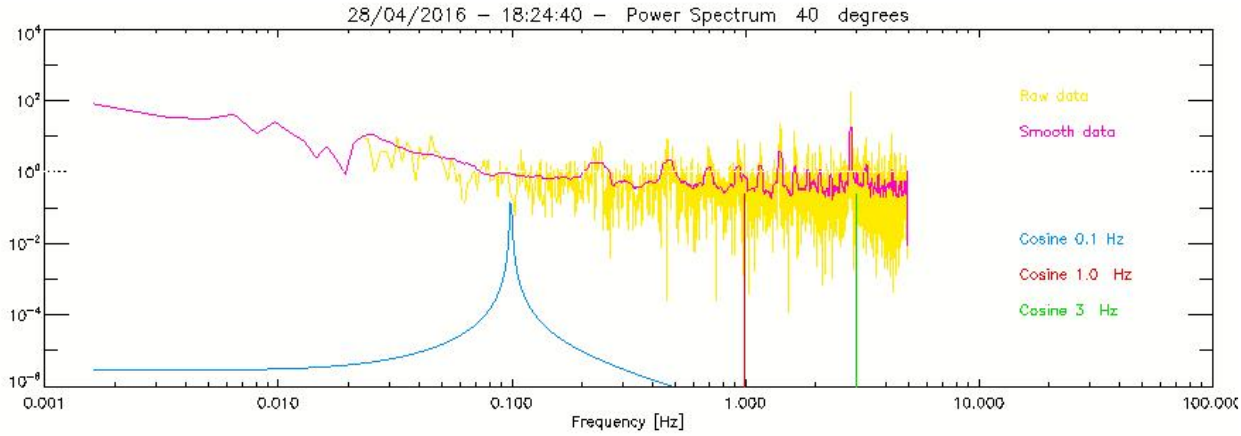

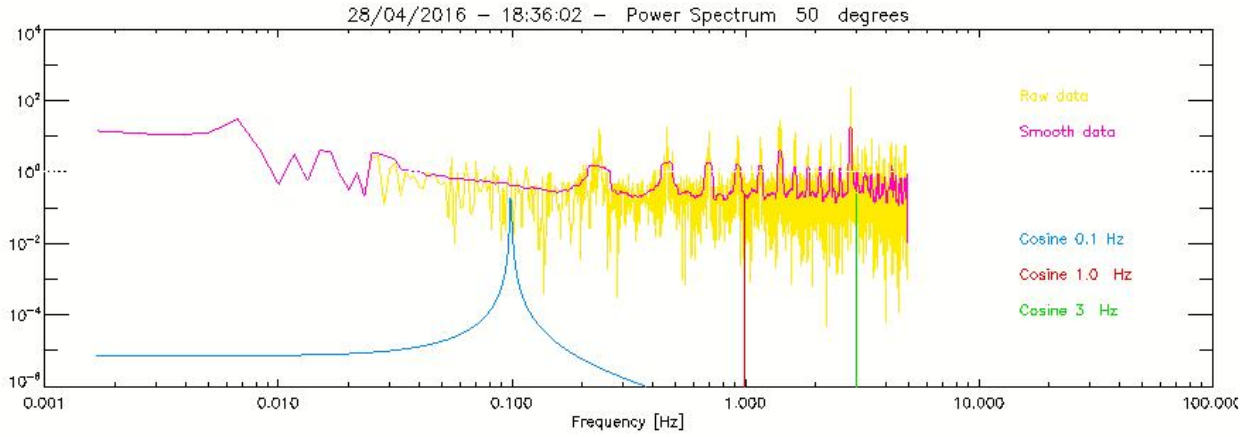

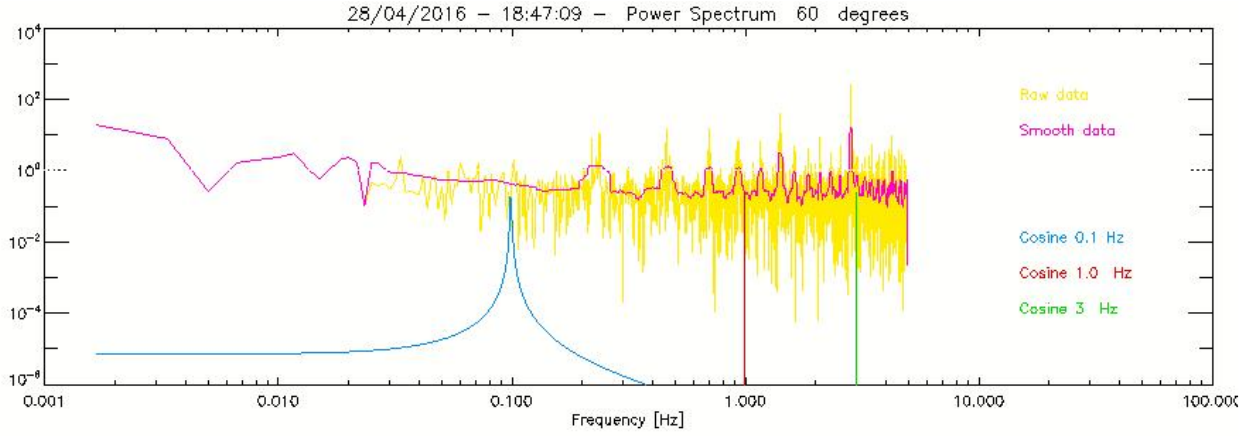

Figures 23 to 26

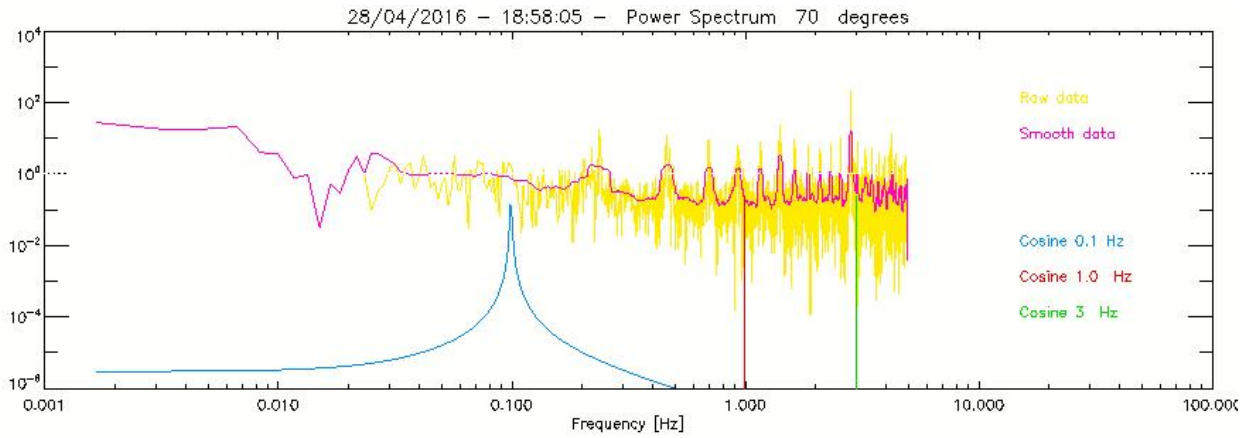

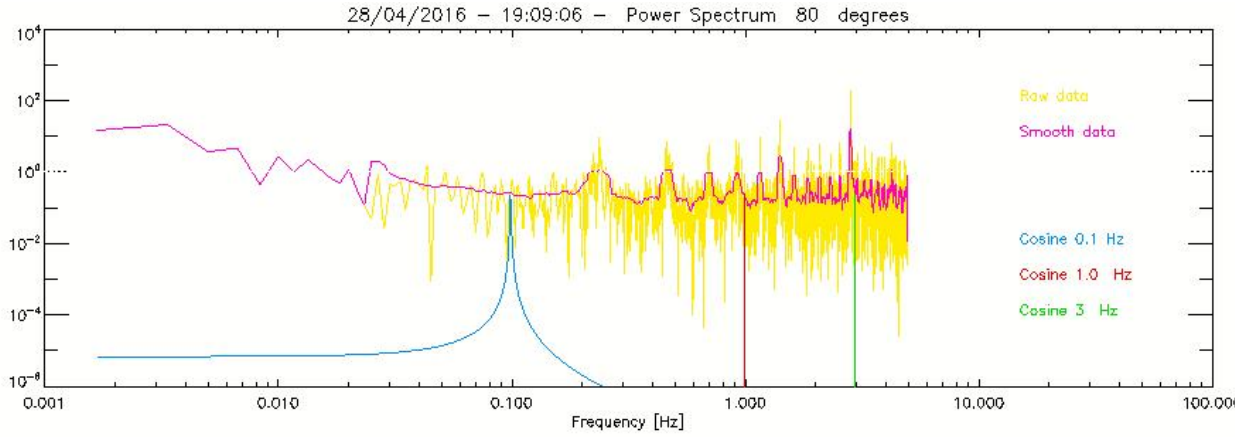

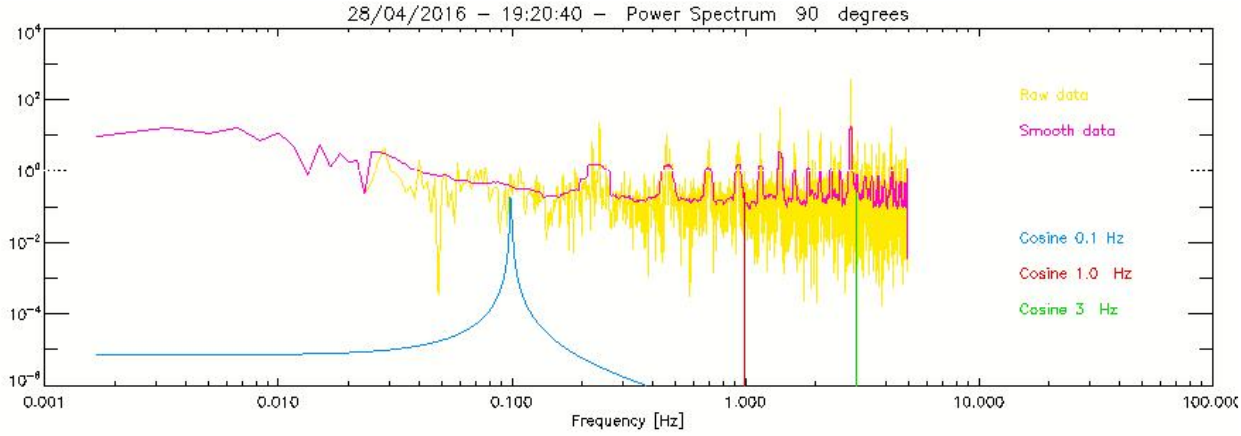

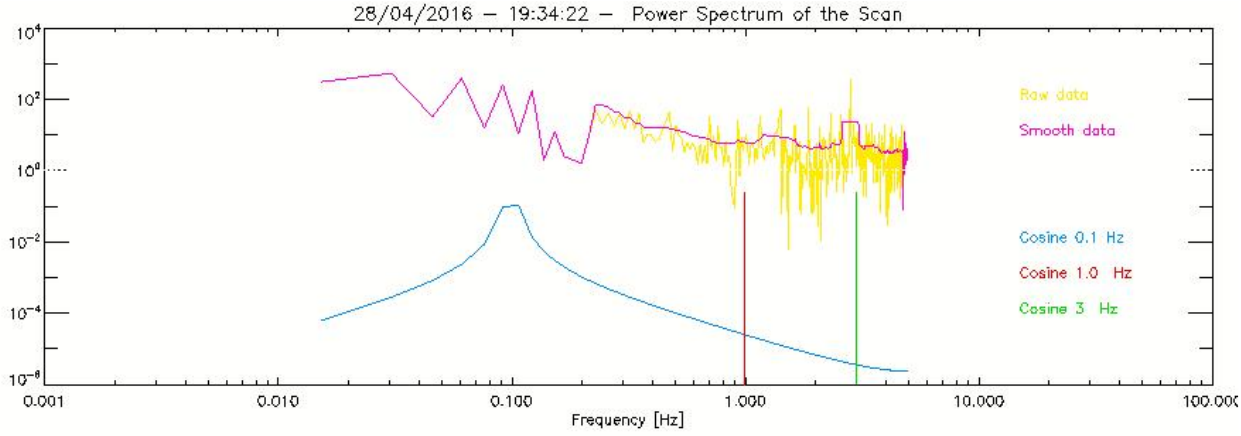

Figures 27 to 30. Figure 30 corresponds to the scan on elevations.

iii. Knee frequency studies

The knee frequency of the power spectrum indicates the time scales above which the correlated variations in the noise introduced by the detector start to dominate. For a given knee frequency f_k , the factor $(1/f_k)$ is such a time scale, that for a time: $t > (1/f_k)$, we will have gain variations in our system which are correlated. That means that they do not average down when we combine more data, as white noise does. This is the wanted 1/f noise. Before this knee frequency, we are dominated by 1/f noise, and after that by white noise.

In the following figures, as illustration of this concept, we are showing the power spectrum of a data set of the QUIJOTE CMB Experiment, with 200 seconds of exposure time, with the knee frequencies found. They are shown with the same presentation criteria.

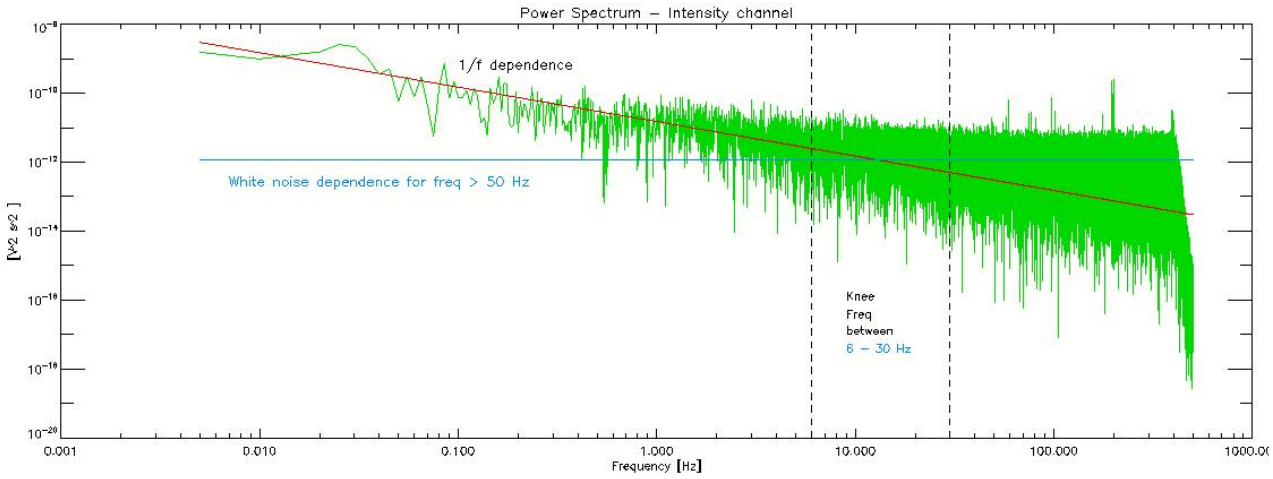

Figure 31: QUIJOTE Intensity Voltage channel - Units are V^2s^2 for power spectra.

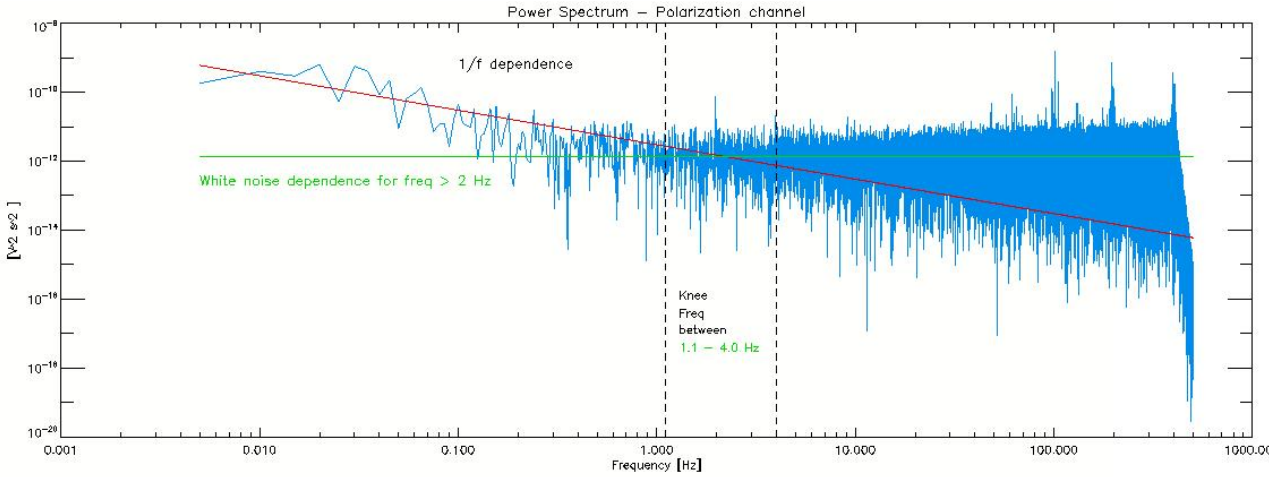

Figure 32: QUIJOTE Polarization Voltage channel - Units are V^2s^2 for power spectra.

For these two figures 31 and 32, the noise power spectrum was fitted as follows. We first divide the sample in two regions, those dominated by 1/f noise and another one dominated by white noise. The white noise level has been fitted as blue and green straight horizontal lines, using frequencies higher than 50Hz and 2Hz, respectively. The 1/f noise region has been added as a line with the 1/f dependence, in red color.. As mentioned above, this noise component follows a frequency dependence of the type $A(1/f)^{\alpha}$. The amplitude A has been chosen according to the power spectrum level; and α was set of 1 as a first approximation. However, I note that for QUIJOTE data, the actual α value is close to 2. With this approximate method, I confirmed that the QUIJOTE knee frequencies are close to their nominal values of 20Hz for the intensity data, and 0.2Hz for the polarization data.

This technique to calculate the knee frequencies at QUIJOTE data sets, was the same used to our antenna's data. This could be presented with any measurement, then I wanted to show the power spectrum of the 80 degrees of elevation data. It is shown with the same presentation criteria than the previous power spectra from QUIJOTE. A straight line in blue color is added to show the Flicker noise dependence, as well another in red color to show the constant dependence of the white noise on the right part of the plot. In order to draw the red line, the average of the last quarter of the spectrum was estimated, where the white noise effect had to be bigger. In this way a knee frequency bigger than 0.1 Hz was found, bigger than the crossing point of the 1/f noise dependence and a estimated level of the white noise. This estimate is affected by the additional sources of noise, as the pile of peaks visible at the smooth data function.

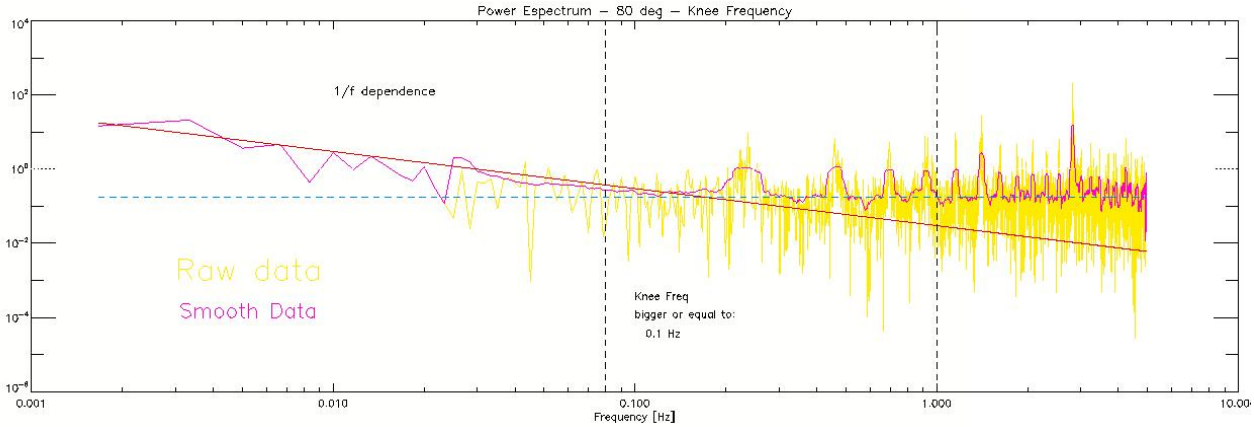

Figure 33: Power spectrum of the data at 80 degrees of elevation, with a knee frequency found bigger than 0.1Hz. A blue dashed line shows the approximate level of the white noise contribution.

$$f_k^{Ant} \geq 0.1\ Hz \qquad \textit{(EQ. 12)}$$

As the peaks shown in the previous plot were understood as a possible electronic contribution, because they appeared well defined in shape, frequency and relevance to the rest of the frequencies, this effect was studied as follows. In order to study these peaks, the following figure was made to show them, and to understand and minimize their effect. The same data file was chosen in order to facilitate the visualization of the plot. Thus:

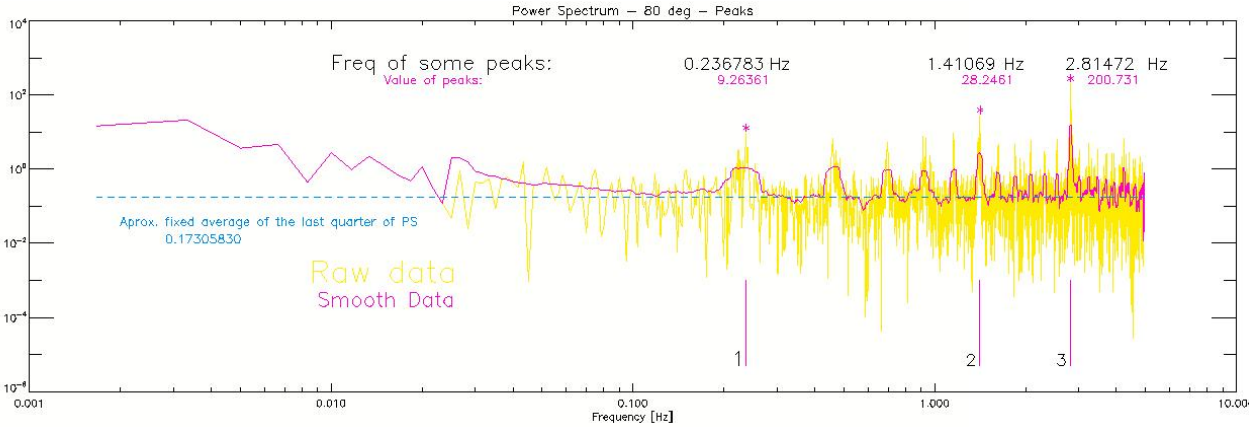

Figure 34: Power spectrum with some peaks highlighted at purple color and asterisks.

An average of the last quarter of the power spectrum, around 0.17 mV^2s^2, is added to show how much relevant those peaks are. When I finally came to the idea of the electronic noise, at the Arduino board, it was easy to make correspond most of them, and harmonics, to different Arduino code parameters.

The code had to take the final analog input, to compare it with the factory built in 2.56V analog reference; and at the end, to write the result on the SD card, along with the automatic measurement of the time. These steps were fully controllable and were designed to work properly, trying to avoid any miscontrol or mistake in the process. Instead, a lot of parameters were arbitrary chosen, and finally resulted as the perfect fit of the new noise contribution.

The peak number 3, at 2.81 Hz, seemed to be associated to the period of blinking at the green status LED attached. In the same way, a digital buffer of 10 measurements was waiting about 1 second to rewrite the text file at the SD card.

To better characterize those electronic noise peaks, an additional measurement was carried out at IAC headquarters on February 10th 2017. The data set was acquired in two measurements of 20 minutes each, and were studied as the previous data. In order to have a blank field direction, an arbitrary northeast azimuth was chosen, as well for the high enough elevation, avoiding the band of geostationary satellites as well as the surrounding buildings.

Following figures 35 and 36 shows the raw data, and later 37 and 38 the power spectrum of each of them, again with cosines as reference:

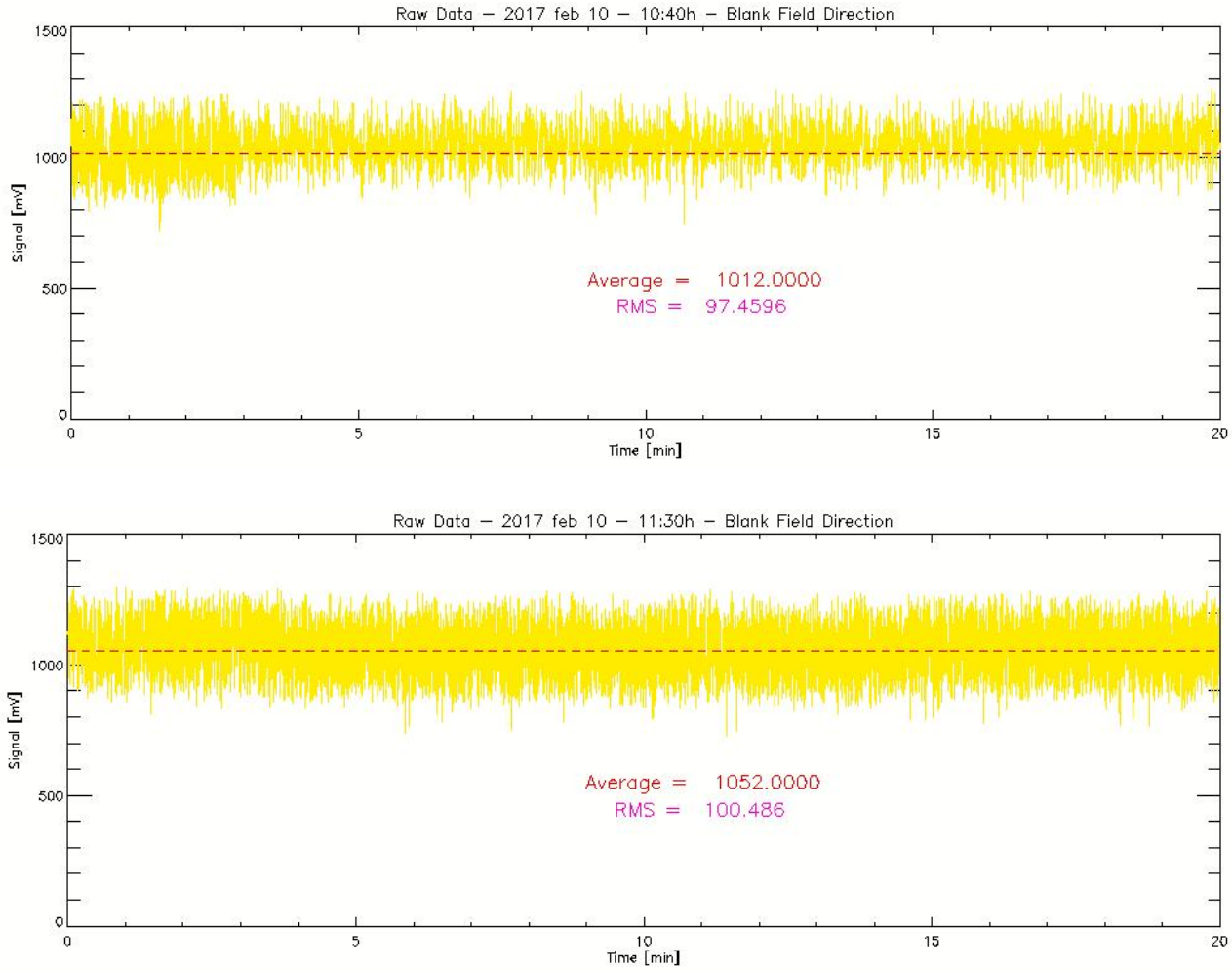

Figures 35 and 36

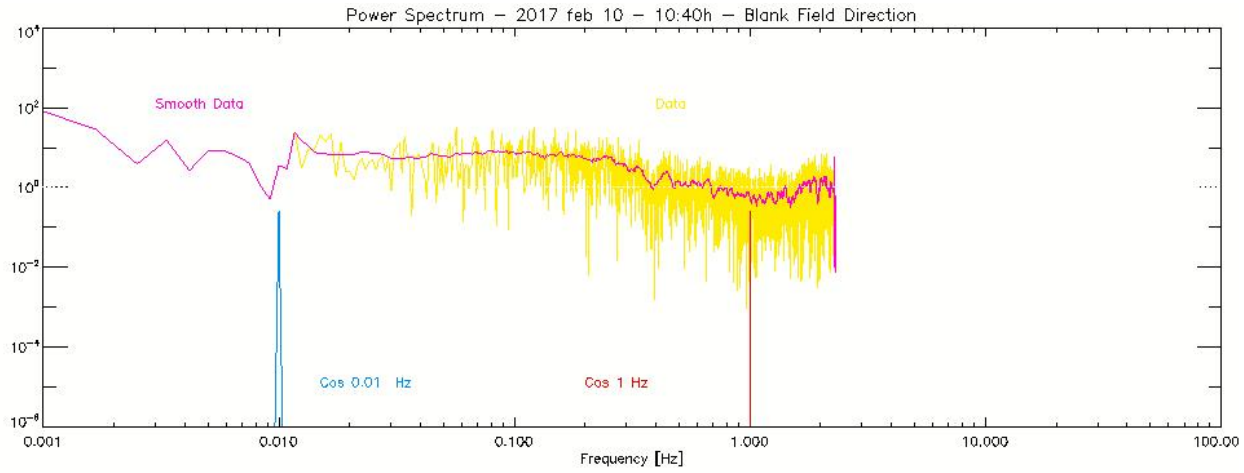

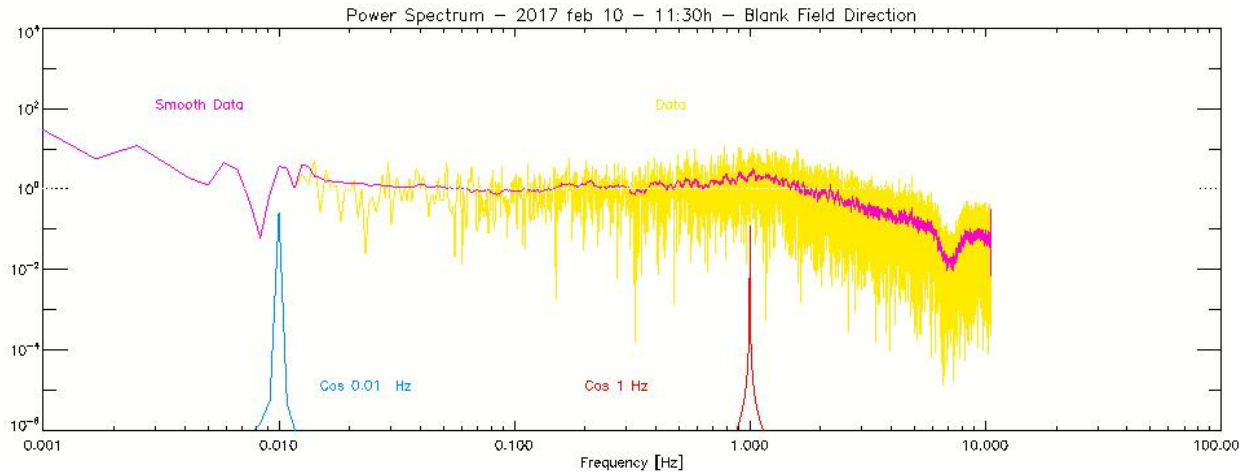

Figures 37 and 38 - Units are mV^2s^2 for power spectra.

In the power spectrum from the 11:30h data, at figure 38, it seems to have an absorption line at around 7.5 Hz. The two spectra are not only non dependent only on the white noise at all, but they can neither be reproduced into the 1/f noise dependence, because they have strong different structures. They are uncomparable to the low noise data from QUIJOTE that we have just seen.

Also although they were taken in a very similar way, their power spectrum are really different, and it was strange from the first moment. They seem to have a different behaviour from the previous spectra, with a not so well defined Flicker noise dependence, and not so dominant white noise one at higher frequencies. Alongside, they are not showing any clear line at 0.01 Hz, where the new rate of SD card saving should show a new peak of electronic noise.

They two were taken after a remodeling of the Arduino voltmeter code, at IAC headquarters on february 10th. The use of the status LED was disconnected, except to warn that the system is ready before measuring, shutting down when starting. Likewise, the saving buffer was changed to accumulate 1000 data, and save them together at the SD card after 100 seconds, at a new rate of 0.01Hz.

No peaks were found in these new sets after the above changes. Even because those different contribution peaks appears together with their harmonic frequencies, mixing all between them and showing us as a line forest of emission peaks. Instead, it was clear enough to realize that there was a lot of electronic noise, in the sets obtained before.

iv. Stability of the gain and noise

In all "ot2" data set taken at Teide Observatory, also at Table 6, the global system was kept advisedly unchanged in order to obtain more data about the behavior of the whole system through a long exposure time. We realized how this mean value was changing from each measurement to any new one; but keeping nearly equal in every one, with an almost imperceptible derivative value of only a few millivolts per minute at each one. Then using Table 6, we got a new global derivative value, measuring the increasing trend of the average value, obtained from those about 2 hours of continuous use time of the system. It resulted in a 2.59 mV/minute value, and can be presented as follows:

$$\frac{|V(t_f)| - |V(t_i)|}{t_f - t_i} = \frac{(1215 - 915)\,mV}{(19:35h) - (17:39h)} \approx 2.59\,mV/min \qquad \textit{(EQ. 13)}$$

This final measure provide us a knowledge of how is evolving the gain and the noise of the system, derived by the inconstant behavior of the global system. Because of the electrical components, not only the heating of the materials and detectors, we have to deal with how be monitoring our evolving system at all times, to actually prevent these effects in the later analysis or at future measurements.

v. Brief study of the antenna sidelobes

Another important result obtained here, is the measure of different deviations from the average of measurements, better to find in the scanning measure, but also visible on the last 2 minutes from measures of 10, 20, 40, 70 and 90 degrees of elevation. On those 2 last minutes I was coming again near to the antenna in order to press off the measuring button. By this way, we can check that there is some signal coming not from the main beam, but from those directions that must correspond to the sidelobes pattern seen on the introduction.

This was easily perceptible thanks to the sound finder, that actually sounded while I was handling something at the radiometer, thus surrounding the antenna position. It was sounding, actually detecting me, but it is not clear in the later data. Only when I did enter almost the central aiming direction, at the main lobe when I was testing without measuring, it was detecting me at sound and likewise at data. It was useful to me, in order to move around the system, and to characterize the use of this antenna system.

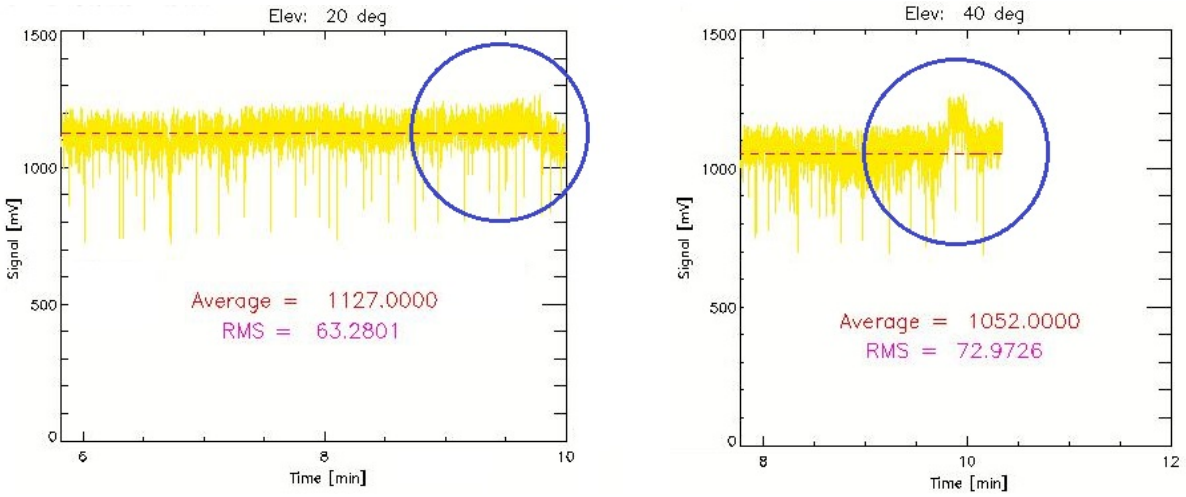

Figure 39: Detail of figures 11 and 13, with the response of the antenna while passing through the sidelobes, highlighted with blue circles, revealing a distortion in the previous constant data.

vi. Atmospheric noise

In order to complete the different origins on the noise results, this kind of elevation measurements could be used to measure the atmosphere contribution, on temperature, into our global noise. With a well noise-controlled measurements, all the data in a chosen file has to show a slight difference from different elevations. Maximal when comparing the zenith direction and the horizon level temperatures; that can provide in its difference the atmosphere's temperature T_{Atm}.

This effect results from the different thickness of the atmosphere due to its air mass and water contained in the layers at the pointing direction of the antenna. Using the following figure we'll see that it has to value less than 10K in our case, and then is too small to be detected with our non cooled and noisy antenna.

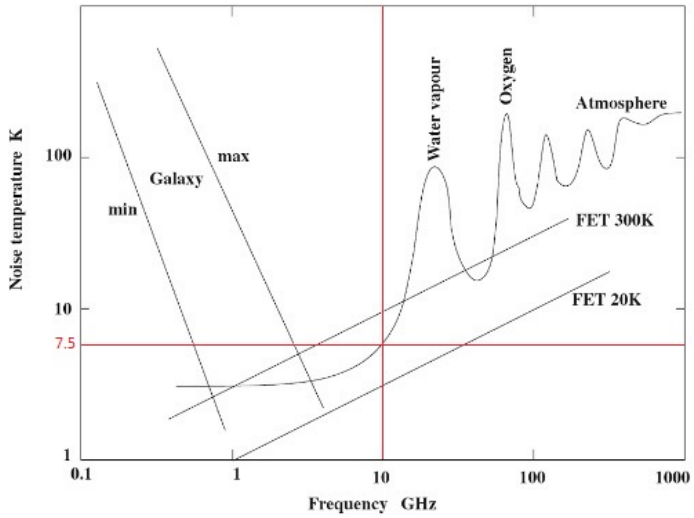

Figure 40: Noise temperature of different components with our 10 GHz frequency and noise level highlighted in red color in a figure taken from "An Introduction to Radio Astronomy" by Burke and Graham-Smith (2010)[9].

Although we could not measure this atmospheric contribution, more than using the second part of the scan on elevations raw data, at figure 20; it guaranteed that we did not are so affected by the atmospheric noise. But the same reason, our expected signal from the atmosphere, less than 7.5 K, will be smaller than our brightness temperature for the Moon case. It resulted in around 10K, as is shown later at the "Calibration of solar temperature measurements" chapter ***d***. It will be important in the case of improved instruments, those so cold that can be sensible to those low temperatures at the same 10 GHz observation frequency.

b. Test of the radiometer equation

The radiometer equation studied at the introduction can be tested with the different sets of data achieved, as well with the QUIJOTE data sets used before. The theory predicts an expected RMS value, determined by the mean value of measurements in our sample <V>, the bandwidth of the instrument Δ_ν , and the sampling rate: τ. This theoretical value has to be compared to the actual value measured in the sample, the calculated RMS. Let's show the collection of parameters for the QUIJOTE data sets, as well for the antenna of the study:

Table 7: Collection of parameters for the radiometer equation

	Mean voltage [mV]	**Bandwidth [Hz]**	**Sampling rate [s]**
QUIJOTE Intensity - channel 1	~ 625	$2 \cdot 10^9$	0.001
QUIJOTE Intensity - channel 2	~ 551	$2 \cdot 10^9$	0.001
QUIJOTE Polarization (Ch.1 - Ch.2)	~ 74.0	$2 \cdot 10^9$	0.001
Antenna (using data at figure 36)	~ 1177	$2 \cdot 10^9$	0.1

Thus we can obtain the expected and calculated values of the RMS, with their corresponding equations, as follows:

$$Theor.\ RMS\ (Ch.1/Ch.2) = \frac{<V>}{\sqrt{\Delta_\nu \tau}}$$

$$Theor.\ RMS\ (Pol) = \sqrt{\left(\sigma_{Ch.1}^{Theo}\right)^2 + \left(\sigma_{Ch.2}^{Theo}\right)^2} \qquad \textit{(EQ. 14)}$$

$$Actual\ RMS = \sqrt{<V^2> - <V>^2} \qquad \textit{(EQ. 15)}$$

And finally show the set of RMS values obtained, given in the following table in order to show and compare them:

Table 8: Theoretical and calculated RMS values

	Theoretical RMS [mV]	**Actual RMS [mV]**	**Exceed**
QUIJOTE Intensity - channel 1	0.442	0.520	17.0 %
QUIJOTE Intensity - channel 2	0.389	0.476	25.1%
QUIJOTE Polarization (Ch.1 - Ch.2)	0.589	0.555	- 6%
Antenna (using data at figure 36)	0.08	56.04	70050 %

Instead of the slight difference between the values for the QUIJOTE cases, we are far apart of the expected value for the RMS. The difference at the QUIJOTE case, can be understood as a consequence of the gain variation at the system. In our case, we are definitely noise dominated. And as studied before, there are a lot of components, mostly electronic noise.

c. Measurement of solar and lunar transits

One of the main objectives of the study was to measure the transit of an astronomical source, in order to characterize the antenna field of view and to carry out a measurement of the solar emission. As we were able to do the first thing, we set out to estimate the Sun's Brightness Temperature at 10 GHz.

i. Correlate time with angular distances in a solar transit

In order to study properly the antenna field of view, we needed to translate those time axis of the measurements, into angular distances. This can be shown and explained looking at the following figure:

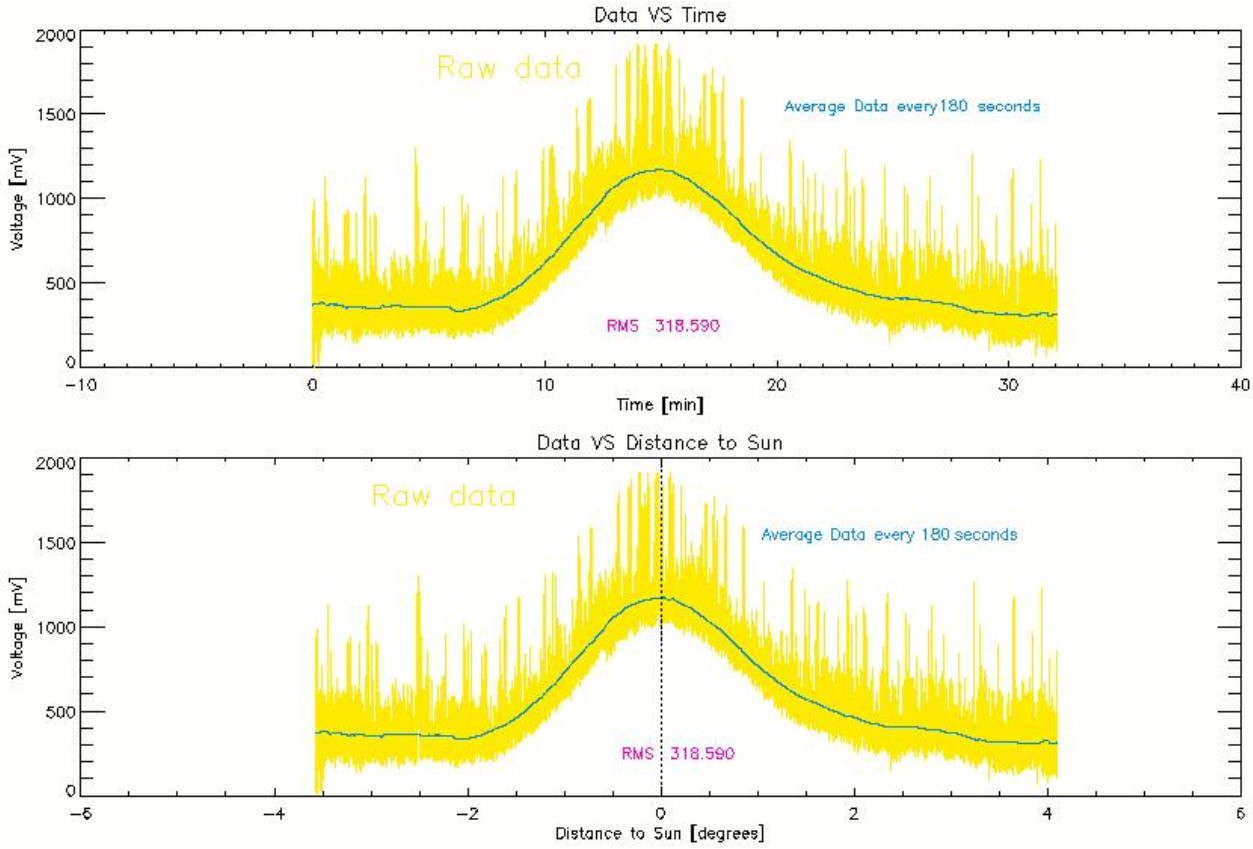

Figure 41: Voltage signal versus time, and distance to the Sun center; as result of the "ot3" measurements at Teide Observatory. An average data set and the RMS are plotted to better see the shape and variation of the data.

In order to get this kind of natural transits, the sun center position was chosen first, and later the antenna is moved, a little bit into the west, about 4 degrees, in 2 degrees twice, which is the smallest movement resolution of the antenna's mount. Then, in order to solve the whole pattern of the transit, one must wait for the sun to move the double of this displacement, a total of about 8 degrees of sky, resulting in about 32 minutes of exposure time.

As we were using an equatorial mount, using the center of the maximum of the transit, and the exact time of each point, we can correlate our time measurements with the exact position of the sun on the sky. With the precise millisecond, when we are at the nearest distance to the solar center position, and the known celestial coordinates; the time is converted into angular distance using that Sun position and the speed of Earth's rotation. Finally, every single time data in the axis is turned into angular distances from the reference point back and forth in the axis.

This is the unique measurement of a solar transit well accomplished. And it also has some problems since the instrument started to malfunction, showing us the voltage data in reverse; as has been previously mentioned. Thus, these plots appear post-corrected with the software in order to show the data.

ii. Measure of the antenna field of view

It was possible to find out the antenna's field of view with that previous solar transit. It can be understood as the full width at the half maximum (FWHM) of the Gaussian distribution that it is showed on this kind of natural transits. With the advice related to the antenna's field of view by Dr. Rubiño, that should be around 3 degrees, 6 times more than the solar disk; I had chosen that previous exposure times, and I had a fundamental basis on the following calibration steps.

Since we are already estimating the behavior of the transit as a Gaussian bell, we must do the same with the data. This Gaussian fit was achieved taking some reference data about this behaviour. Some of them are: the center position of the bell, the amplitude, and the base level, if it is not zero. The rest of parameters, as a linear o quadratic dependences, are not taken into account due to the previous near constant behaviour of the response.

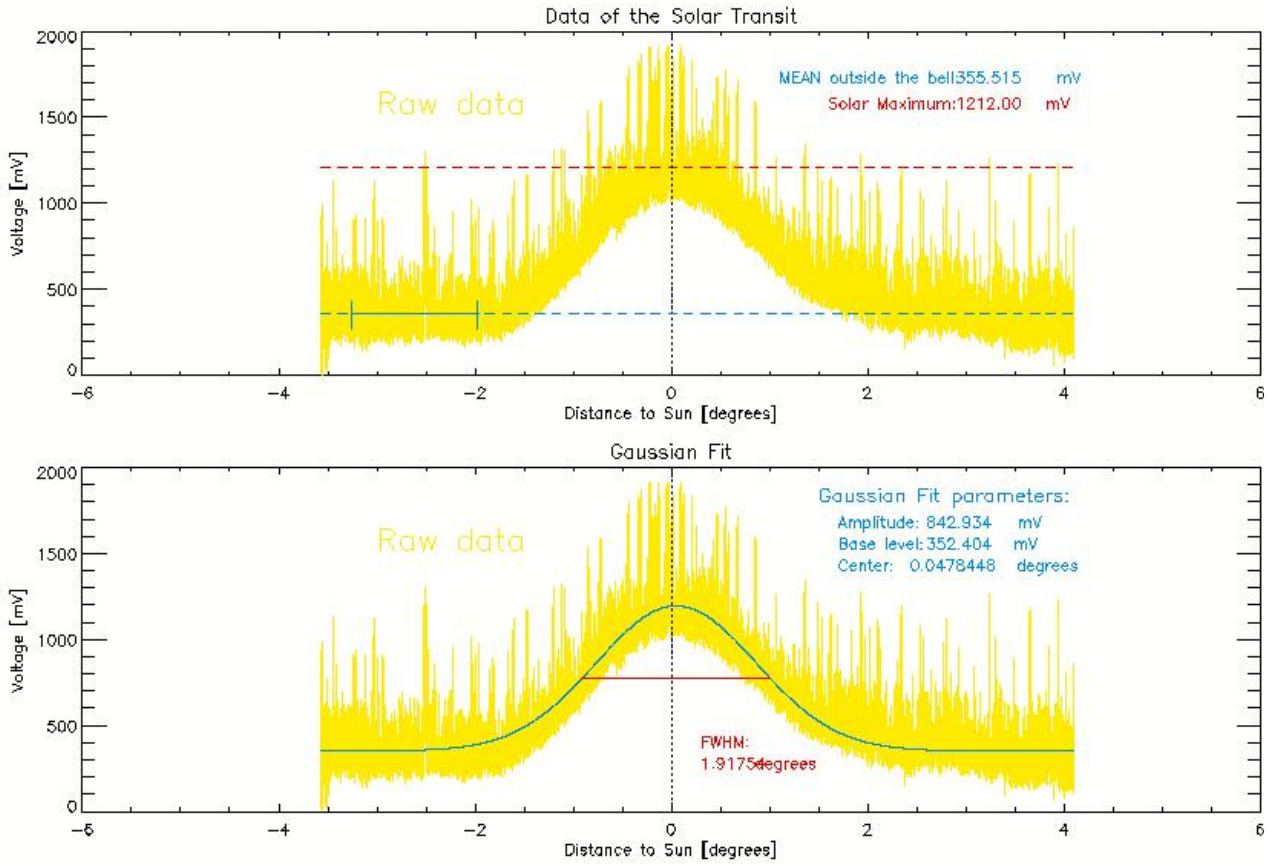

Figure 42: In the upper section it is shown the approximations to gaussian levels.
Lower there is the gaussian fit with result parameters, and FWHM.

The previous figure shows all these considerations: The amplitude was taken as the subtraction of the level outside the bell, to the maximum of the solar emission. And that base level could be anyone, and was well defined in this case. For the center was taken the zero value, as we were working on a centered gaussian, in terms of distance to the Sun. The FWHM resulted in a value of 1.9175 degrees, our wanted antenna's field of view.

Table 9: Gaussian fit parameters

	Amplitude [mV]	Base level [mV]	Center [degrees]	FWHM [degrees]
Result of the fit	842.9	352.4	0.05	1.92

d. Calibration of solar temperature measurements

The final part of the study consisted in the reliable measurement of solar effective temperature at our microwaves frequencies. As described in the introduction, we can know precisely the Moon temperature on our bandwidth and by this way use it to calibrate solar emission saved into our data, comparing them with the Moon data acquired at almost the same moment; maintaining the operational properties on our antenna's system.

i. Fundamentals of the calibration method

In the antenna fundamentals introduction we had learnt that what is measured directly is the voltage difference from a baseline, also offset level, but leveled by a given and regulated gain. This voltage is related to the antenna temperature by the gain as follows:

$$V = G \cdot T_{Sys} \qquad \textit{(EQ. 16)}$$

If we have in addition the approximation of having a solid angle subtended by our antenna, much larger than the subtended solid angle of our source (for both Sun and Moon, having a similar size):

$$\Omega_{Antenna} \gg \Omega_{Source} = \Omega_{Sun} \simeq \Omega_{Moon} \qquad \textit{(EQ. 17)}$$

We can arrive at the interpretation of getting that the antenna temperature is equivalent to that of the Sun but diluted in the quotient of the angles that both subtend; resulting in:

$$T_{Ant,\,Source} \simeq \frac{\Omega_{Source}}{\Omega_{Ant}} \cdot T_{B,\,Source} \qquad \textit{(EQ. 18)}$$

And just with a the expression of the proportion of voltages of the Sun and Moon, we would get the calibrated measure of the Sun's temperature from the Moon's:

$$\frac{\Delta V_{Sun}}{\Delta V_{Moon}} = \frac{T_{Ant,\,Sun}}{T_{Ant,\,Moon}} = \frac{T_{B,\,Sun}}{T_{B,\,Moon}} \cdot \frac{\Omega_{Sun}}{\Omega_{Moon}} \simeq \frac{T_{B,\,Sun}}{T_{B,\,Moon}}$$

$$\Rightarrow \quad T_{B,\,Sun} \simeq T_{B,\,Moon} \cdot \frac{\Delta V_{Sun}}{\Delta V_{Moon}} \qquad \textit{(EQ. 19)}$$

ii. Methodology of the calibration measurements

Instead of comparing long data files got from lunar and solar emissions in different sequential transits with the radiometer, we used a previous method, comparing Sun and Moon radiation, point to point in single data acquisitions. This kind of comparisons were only made in 18th December 2015. The system was used with an oscilloscope in order to have data from the final millivolts signal. At that moment, was necessary to use a live comparison of maximum lunar emission with maximum solar emission in order to do it.

Once the antenna is placed and set up pointing to the celestial North, it is placed at the object and its surrounding sky successively, using the mount for aiming and guiding and the sound finder for accurate positioning. All for both Sun and Moon cases. This method implies to be subtracting all the sky measures to the previous aimed object, making them successively in order to avoid any change in the antenna's response, bigger than the expected global derivative value studied, as seen previously.

iii. Data of calibration measurements

A good relation was found using this method, with a roughly reasoned measurement of about 11300K at the Sun, like the expected from Zirin et al. (1991)[1] for our 10 GHz frequency. Data summary achieved is on following tables.

In the case of the Moon, we hope the blackbody temperature predicted by the phase variation model by Gorenstein and Smoot (1981)[2], seen on section d. Near to 202K, it was calculated for the two dates of measurements, as follows:

Table 10: Moon temperature from the Gorenstein and Smoot[2] model (eq. 04)

Date	Phase angle [deg]	T(Moon) [K]
Dec 18th 2015	269.5 ± 0.1	**201.7 ± 7.5**
Feb 4th 2017	263.0 ± 0.1	**198.7 ± 7.5**

Table 11: Comparative measurements of the Sun and the Moon

Date	**ΔV Sun [mV]** (center - surroundings)	**ΔV Moon [mV]** (center - surroundings)
Dec 18th 2017	545 - 286 = **259 ± 0.5**	280 - 275 = **5 ± 0.5**

The set of measurements taken at Teide National Park outer limit, on February 4th, was impossible to use, as they were not good enough to discriminate the Moon signal over the base level. This was also the last clue to realize that it was not a problem on the radiometer electronics, as the amplification or Arduino boards failing, working in reverse; but it had to be something never changed until that final measure. This problem resulted in the reverse malfunction mentioned, but also in an important loss of the system gain at the first steps of the electronics, where no signal have been already measured, pointing to the LNB detector, if not the portable oscilloscope when measuring.

As we have seen, the calibrated results will depend on the proportion between the solid angle of the source, the Moon or the Sun, and the solid angle of our antenna. For the Moon and Sun, a circle approximation was used for their solid angles, as $\mathbf{\Omega}_S=\pi r_S^2$, taking their respective visual angles at the date of the data. For the antenna, like the FWHM at a gaussian distribution corresponds to: $FWHM=\sigma\sqrt{8}\ln 2$ we can assume a $\mathbf{\Omega}_A=2\pi\sigma^2$ and then take it in terms of the calculated FWHM at the gaussian fit. Using them to get the proportions of solid angles, we have:

$$\Omega_{Sun} = 0.0002808\ sr \qquad \textit{(EQ. 20)}$$

$$\Omega_{Moon} = 0.0002756\ sr \qquad \textit{(EQ. 21)}$$

$$\Omega_{Ant} = 0.0012691\ sr \qquad \textit{(EQ. 22)}$$

Where the equation 17 is verified, as $\mathbf{\Omega}_{Antenna}$ is much greater than $\mathbf{\Omega}_{Source}$ for both cases.

iv. Results of Sun temperature

We want to characterize the system with the data from December 18th 2015. Using the previously seen equation 18, we can obtain the Sun temperature at 10 GHz from its antenna temperature as:

$$T_{Sun}\,[K] = \frac{\Omega_{Ant}}{\Omega_{Sun}} \cdot T_{Ant}^{(Sun)} \qquad \textit{(EQ. 23)}$$

We change now that antenna temperature for the Sun, in terms of the one obtained from the Moon, as equation 19:

$$T_{Sun}\,[K] = \frac{\Omega_{Ant}}{\Omega_{Sun}} \cdot T_{Ant}^{(Moon)} \cdot \frac{\Delta V_{Sun}}{\Delta V_{Moon}} \qquad \textit{(EQ. 24)}$$

And finally considering that this antenna temperature from the Moon is the dilution into our beam of the calibration temperature of the Moon at 10 GHz, found with the Gorenstein and Smoot (1981)[2] model, we arrive at the final result of the Sun temperature:

$$T_{Sun}\,[K] = \frac{\Omega_{Ant}}{\Omega_{Sun}} \cdot \left[\frac{\Omega_{Moon}}{\Omega_{Ant}} \cdot T_{Moon}\,[K]\right] \cdot \frac{\Delta V_{Sun}}{\Delta V_{Moon}}$$

$$T_{Sun}\,[K] = \frac{\Omega_{Moon}}{\Omega_{Sun}} \cdot \frac{\Delta V_{Sun}}{\Delta V_{Moon}} \cdot T_{Moon}\,[K] \qquad \textit{(EQ. 25)}$$

$$T_{Sun}\,[K] = \frac{0.0002756}{0.0002808} \cdot \frac{259 \pm 0.5}{5 \pm 0.5} \cdot (201.7 \pm 7.5)\ K$$

$$T_{Sun}\,[K] = 13669 \pm 1367\ K$$

Although this measurement was the only one acquired, it was close to the expected 11300 K from Zirin et al. (1991)[1].

4. CONCLUSIONS

This study has been taken to characterize commercial antennas for scientific purposes and as a testbench of the available technology. Both aspects have produced clear conclusions while, on the other hand, some data has been lacking in the study to specify certain issues in other cases. Here there the main achievements:

4.1 An antenna system has been developed with an expressly designed radiometer.

4.2 It has been measured the antenna's main power pattern, with the field of view rounded to 1.92 degrees.

4.3 The antenna's noise properties have been weighted.

4.4 A calibrated measurement of the Sun Temperature was taken. We obtain 13669 ± 1367 K, on Dec 2015. This value is consistent with the study from Zirin et al. (1991)[1] and compatible with a quiet Sun state.

Other qualitative results were also found. Thanks to them, we are provided of more tools in order to achieve better data sets, likewise improve the methods used in the study. Some are:

4.5 An upper limit to the atmospheric noise contribution.

4.6 An illustration of the relevance of the sidelobes.

4.7 The important electronic noise found in the study and the way to solve it.

5. FUTURE WORK

Despite the already mentioned reverse malfunction, that affects the LNB first detector to check, a normal system usage was possible. Thus, a lot of improvements can be develop to get forward into more measurements of the solar radio emission. As long as this antennas can be combined with other powerful complements, engineering can provide a lot of new appliances reaching new levels on astronomical research, possibly at all levels, not limited to use at this physics degree university level. The following are some of the aspects to improve:

1. Due to malfunction experienced with the radiometer in this study, a complete revision of its components is required, or at least an improved redesign based on the materials used in the study. A stable power supply, as rechargeable batteries, would make the radiometer noise independent of the main electrical sources.

2. Whenever a renovated radiometer exists, a set of replay measurements have to be developed to confirm such a wide collection of results.

3. At the Arduino code, a methodical debug of the code is also necessary, in order to properly set up the board to work as a better voltmeter, or to use the main built-in capabilities, as run its own linux-based OS to do the data reduction after the recordings, and to save the raw data and first processed results automatically to the cloud, vía WiFi connection. The WiFi would have to be used when it is not measuring, avoiding in this way any interferences in our observation band.

4. A stable settlement with a fully available pillar and mount, at any location, would help to obtain the measurements, and maintain their stability, and could extend this study to the noise properties at that location. A portable configuration of the antenna dish would also help to set and unset up the whole system.

5. There could be an "Introduction Sheet" for outreach purposes, in which it can be explained how to set up and manage the system, show some antenna fundamental concepts, as well show the main science that can be done, or a variety of scientific dissemination curiosities.

With the development of some of these improvements, besides the techniques applied in this study, a new settlement of basic radioastronomy and its instrumentation, at university level, has been set. A master degree program could arrange somehow a new lection on astrophysical techniques, to develop and demonstrate the science here described.

People and Acknowledgments

I want to write down the list of people who gave me the strength and appropriate behaviour to complete this study, and all the surrounding things that it entails, from december 2015 until february 2017.

- First to my girlfriend Noe Herzog for all her endurance and integrity in all deals with me along all this time. In the same way to my IAC teacher Alberto Rubiño, who also showed me the best way to write a scientific study, although this work may not do justice to that.

- Thanks to the related IAC members; Alfred Rosenberg and Roger Hoyland, for their technical and logistical support. A special thanks to Juan José Sanabria, TOT from Teide Observatory for his support on the continuous development and constant help with the Arduino board and code.

- Also to all rest of IAC members involved, as Abelardo, Higinio, Panchi, Laura, Laia, Yaiza and Fina, and a lot of students who gave me the needed strength to fulfill this study as long I was studying my last Quantum Mechanics exam. Thanks to Josafat, Alejandro, Rafa, Klaus, Björn Soergel, Alberto Bueno, Ana Griñón, Adur Pastor and many others. But most special thanks to Cassiopeia members and friends: Josep, Rodrigo, Andrea, Isaac, Salva and Lucas.

- Finally, I want also to keep my teammates in mind. The people who shouldered me even from their unrelated positions. I want to thank Miguel, Óscar and Juanjo Martín from Discover Experience, Oswaldo and Rubén from Museos de Tenerife, and also to Ana, Macarena, Adeline, Eduardo, and Jaime from Volcano Teide. I don't want to miss Carmelo from AstroTour for his special kind of support. And a great and special thanks to Eric from Cosmos

Tenerife for his help at Teide with his time and electric generator!

References and Bibliography

[1] Zirin, H., Baumert, B. M., Hurford, G. J. *The microwave brightness temperature spectrum of the quiet sun* (1991).

[2] Gorenstein M. and Smoot G., *Ap.J. volume 244, 361* (1991).

[3] Hagfors T., *Remote probing of the moon by infrared and microwave emission and by radar* (1970).

[4] Krauss, J.D., *Radio Astronomy* (1966).

[5] Rubiño A., *An Interferometric Study of the Cosmic Microwave Background Anisotropies* (2002).

[6] Harrison D., Rubiño A. et al., *A measurement at the first acoustic peak of the CMB with the 33 GHz interferometer* (2000).

[7] NRAO, *Essential Radio Astronomy* Course. www.cv.nrao.edu/course/astr534/ERA.shtml

[8] ESA, *Advanced Synthetic Aperture Radar (ASAR) user guide*. https://earth.esa.int/handbooks/asar/CNTR5-2.html

[9] Bernard F. Burke and Francis Graham-Smith, *An Introduction to Radio Astronomy* (2010). https://goo.gl/g1YJFI

[10] Stanford University School of Engineering, *Noise in Antennas*. http://web.stanford.edu/class/ee252/handouts/antenna_noise.pdf

[11] Wienand J., *Propagation of uncertainty calculator (Error Analysis)*. http://julianibus.de/physik/propagation-of-uncertainty

[12] Cardiff University, *Background to Radio Astronomy.* https://www.astro.cf.ac.uk/observatory/radiotelescope/background/

[13] Arduino International Project, *Yún Board Specifications* https://www.arduino.cc/en/Main/ArduinoBoardYun

[14] Chat Hull, student at UC Berkeley, *The Radiometer equation* https://www.youtube.com/watch?v=dwT-tMoscsY

[15] Wikipedia, *Schumann resonances* https://en.wikipedia.org/wiki/Schumann_resonances

[16] Astronomical Applications Department of the U.S. Naval Observatory http://aa.usno.navy.mil

HERNANDEZ GARCIA ADRIAN - 78630522P

Firmado digitalmente por HERNANDEZ GARCIA ADRIAN - 78630522P
Nombre de reconocimiento (DN): c=ES, serialNumber=78630522P, sn=HERNANDEZ GARCIA, givenName=ADRIAN, cn=HERNANDEZ GARCIA ADRIAN - 78630522P
Fecha: 2017.03.03 13:55:14 Z

ANNEX 1: List of tables

ANNEX 2: List of figures